Calcolo (2017) 54:471–501
DOI 10.1007/s10092-016-0194-z

On the grad-div stabilization for the steady Oseen and Navier-Stokes equations

Naveed Ahmed[1]

Received: 11 January 2016 / Accepted: 7 June 2016 / Published online: 21 June 2016

Abstract This paper deals with the choice of stabilization parameter for the grad-div stabilization applied to the generalized Oseen equations. In particular, inf-sup stable conforming pairs of finite element are used to derive the stabilization parameter on the basis of minimizing the $H^1(\Omega)$ error of the velocity. For the proposed choice of the parameter, the $H^1(\Omega)$ error of the velocity is derived that shows a direct dependence on the viscosity coefficient. Differences and common features with the Stokes equations are discussed. Numerical studies are presented which confirm the theoretical results. Moreover, for the Navier-Stokes equations, numerical simulations are performed on a two-dimensional flow past a circular cylinder. It turns out that, for the MINI element, the best results are achieved without grad-div stabilization.

Keywords Incompressible Navier-Stokes equations · Mixed finite elements · Grad-div stabilization · Error estimates · Stabilization parameter

Mathematics Subject Classification 35Q30 · 76M10 · 65L60

1 Introduction

Incompressible flows are modeled by the incompressible Navier-Stokes equations

$$\begin{cases} -\nu\Delta\mathbf{u} + \mathbf{u}\cdot\nabla\mathbf{u} + \nabla p = \mathbf{f} & \text{in } \Omega, \\ \nabla\cdot\mathbf{u} = 0 & \text{in } \Omega, \\ \mathbf{u} = \mathbf{0} & \text{on } \partial\Omega. \end{cases} \tag{1}$$

✉ Naveed Ahmed
ahmed@wias-berlin.de

[1] Weierstrass Institute for Applied Analysis and Stochastics, Leibniz Institute in Forschungsverbund Berlin e. V. (WIAS), Mohrenstr. 39, 10117 Berlin, Germany

Here, $\mathbf{u}$ is the velocity, p the pressure, $\mathbf{f}$ represents body forces, $\Omega \subset \mathbb{R}^d, d = 2, 3$ is a domain, $\partial\Omega$ is the boundary of Ω, and ν is the kinematic viscosity. In high Reynolds number flow problems, i.e., $\nu \ll 1$, a stabilization of the Galerkin finite element formulation is necessary. A popular remedy is to add a term based on the streamline upwind Petrov-Galerkin (SUPG) [1] to the finite element formulation that accounts for stabilizing dominating convection. However, a main difficulty in the analysis of the SUPG method comes from the coupling between velocity and pressure. It is suggested in [2,3] that an additional stabilization, the so called grad-div stabilization, is important for the robustness.

The grad-div stabilization is also used as an efficient tool to improve the conservation of mass and to reduce the velocity error caused by the pressure error in the simulations of incompressible flow problems. In the finite element formulation, the grad-div term, which is based on the residual of the continuity equation, adds the stabilizing term $\gamma(\nabla\cdot\mathbf{u}_h, \nabla\cdot\mathbf{v}_h)$ to the momentum equation. Such a term also occurs in the subgrid pressure model in the framework of scale separation of variational multiscale formulations of the Navier-Stokes equations [4,5].

The grad-div stabilization term is studied at several places in the literature for the simulation of incompressible flow problems. In [6], it is proposed for the Stokes problem. It is shown that the addition of the grad-div term improves the well-posedness of the continuous problem for small values of the viscosity. Moreover, the influence of stabilization term on the accuracy of the solution is analyzed. The application of the grad-div stabilization term for the rotational form of the Navier-Stokes equation can be found in [7]. It is shown numerically that the difference between the skew-symmetric and the rotational form of the nonlinearity is due to the increased error in the Bernoulli pressure, which in turn increases the velocity error. The use of the grad-div stabilization ameliorates the effect, especially for high Reynolds number, and thus reducing the error in the velocity field. Numerical studies presented in [8] also shows that the grad-div stabilization is useful for practical application of some turbulence models. In [9], a combination of the SUPG and grad-div stabilization methods are studied for the generalized Oseen equations. It was concluded that the SUPG method is less important for the inf-sup stable pair of velocity and pressure due to the constant in the stabilization parameter which depends on the problem data. The authors also shows that the numerical instabilities occur for slightly distorted quasi-uniform meshes. Furthermore, considering only the grad-div stabilization, it is acknowledged that the grad-div stabilization is more important and leads to satisfactory results.

The analysis of the grad-div stabilization in combination with the finite difference time stepping schemes applied to the transient Oseen problem is presented in [10]. The analysis is based on the use of the specific Stokes projection. The authors perform the analysis for the semi-discrete and for the fully discrete problem. They prove the optimal error bounds for both velocity and pressure for sufficiently smooth solutions with constants that do not depend on the viscosity. In [11], for the transient Oseen problem, the local projection stabilization together with the grad-div stabilization was considered.

The choice of the stabilization parameter γ in the grad-div stabilization is important for accuracy, however, a conflicting interest can be the choice of γ for ease in solving

Schur complement problem [12,13]. The advantage of the grad-div stabilization in preconditioning is its positive effect in the solution of the Schur complement problem.

The primary objective of this paper is to study the choice of optimal parameter γ for the grad-div stabilization in mixed finite element methods for the Oseen and Navier-Stokes equations (1).

Theoretical analysis and numerical simulations performed for inf-sup stable pairs of elements, see e.g., [14–16], indicate that $\gamma = \mathcal{O}(1)$ is often a good choice. Further, considering only the grad-div stabilization in [9], it is demonstrated that the optimal parameter should be chosen $\gamma = 10^{-1}$. A theoretical analysis proposed in [17] also suggests that the stabilization parameter should be $\mathcal{O}(1)$ for inf-sup stable elements. However, in [18] it is shown that an optimal γ can be much larger than $\mathcal{O}(1)$ in certain situations, depending on the size of the pressure relative to that of the velocity. Furthermore, for solutions with large or complicated pressures, good results are obtained with $\gamma = 10^4$ whereas the bad results are obtained with $\gamma = 1$ or 10.

A detailed investigation of the optimal grad-div stabilization parameter γ in mixed finite element methods for the Stokes equation can be found in [19]. The optimal parameter is obtained by minimizing the $H^1(\Omega)$ error of the velocity and $L^2(\Omega)$ error of the pressure. It is demonstrated that this choice depends on the magnitude of the pressure relative to that of the velocity in the appropriate norms. However, it is independent of the viscosity and pressure if an appropriate stabilization parameter is used and a point-wise divergence-free subspace with optimal approximation space exists. Moreover, it is also established that a good choice of the stabilization parameter for minimizing the $H^1(\Omega)$ velocity error compared to the $L^2(\Omega)$ error of the pressure gives larger parameter.

The main contribution of this manuscript is the extension of the idea presented for the Stokes problem in [19] to the Oseen equations which can be seen as a direct linearization (fixed point iteration) of the steady-state or time-dependent Navier-Stokes equations. For the sake of brevity, the minimization of $H^1(\Omega)$ error of velocity is taken into account for finding the optimal parameter in the grad-div stabilization. The results are obtained by considering the $H^1(\Omega)$ velocity error as a function of γ and then minimizing it. It is concluded that the stabilization parameter γ, depending on the situation that whether or not the point-wise divergence-free subspace of the velocity space has optimal approximation properties, might be of different size. The optimal parameter depends on the norms of the velocity and pressure and the element choice, and might depend on the reaction coefficient σ, the mesh width h, and the viscosity ν. For example, the optimal γ depends on the mesh width h for the MINI element whereas this is not true for the Taylor-Hood element. Similar observations have been made in the Stokes problem [19]. The insertion of the proposed stabilization parameter γ into the error estimates leads to a ν-dependent error bound irrespective of the optimal approximation properties of the divergence-free subspace of the velocity space. This is in contrast to the Stokes problem, where the dependence of the error on ν is only for those cases where the point-wise divergence-free subspace of velocity does not have optimal approximation properties.

The numerical simulations for the steady-state flow around a circular cylinder suggest, using the MINI element on standard as well as on Delaunay type grids, that the grad-div stabilization is not always useful to improve the accuracy of the com-

puted solution. Furthermore, the use of inf-sup stable Taylor-Hood finite element with optimal parameter leads to accurate results when compared to the reference data [20].

The remainder of the paper is organized as follows: Sect. 2 introduces the generalized Oseen equations and its continuous and discrete formulation. Moreover, the spaces of divergence-free and discretely divergence-free functions are given. In Sect. 3, error estimates based on the minimization of the $H^1(\Omega)$ error of the velocity are presented, which render suitable parameter choices for the stabilization parameter γ. Section 4 gives some numerical tests thereby substantiating the appositeness of the theoretical results. It is shown that, depending on the finite element space and the mesh, the optimal parameter vary from $\mathcal{O}(h^2)$ to $\mathcal{O}(10^4)$. A similar observation can be found in [19]. The paper is concluded with a summary of the results.

2 A linearized Navier-Stokes problem

Consider the generalized Oseen problem, as a model problem for linearized Navier-Stokes equations, in its most general form as

$$\begin{cases} -\nu\Delta\mathbf{u} + \mathbf{b}\cdot\nabla\mathbf{u} + \sigma\mathbf{u} + \nabla p = \mathbf{f} & \text{in } \Omega, \\ \nabla\cdot\mathbf{u} = 0 & \text{in } \Omega, \\ \mathbf{u} = \mathbf{0} & \text{on } \partial\Omega, \end{cases} \tag{2}$$

with constants $\nu > 0$, $\sigma \geq 0$ and a known convection field $\mathbf{b} \in L^\infty(\Omega)^d$. The cases $\sigma = 0$ and $\sigma > 0$ are considered separately for the simplicity of the presentation.

Throughout this paper, the standard notation for Lebesgue and Sobolev spaces is used. The L^2 inner product in a domain Ω is denoted by $(\cdot,\cdot)$ and the corresponding norm is denoted by $\|\cdot\|_0$.

Let the function spaces for velocity and pressure be $V := H_0^1(\Omega)^d$ and $Q := L_0^2(\Omega)$, respectively. Then, the variational formulation of (2) reads: find $(\mathbf{u}, p) \in V \times Q$ such that for all $(\mathbf{v}, q) \in H_0^1(\Omega)^d \times L_0^2(\Omega)$

$$\begin{cases} \nu(\nabla\mathbf{u}, \nabla\mathbf{v}) + b_s(\mathbf{b}; \mathbf{u}, \mathbf{v}) + \sigma(\mathbf{u}, \mathbf{v}) - (\nabla\cdot\mathbf{v}, p) = (\mathbf{f}, \mathbf{v}), \\ (\nabla\cdot\mathbf{u}, q) = 0, \end{cases} \tag{3}$$

where the bilinear form b_s is defined by

- $b_s(\mathbf{b}; \mathbf{u}_h, \mathbf{v}_h) = (\mathbf{b}\cdot\nabla\mathbf{u}_h, \mathbf{v}_h)$ with $\nabla\cdot\mathbf{b} = 0$,
- $b_s(\mathbf{b}; \mathbf{u}_h, \mathbf{v}_h) = \frac{1}{2}\big\{(\mathbf{b}\cdot\nabla\mathbf{u}_h, \mathbf{v}_h) - (\mathbf{b}\cdot\nabla\mathbf{v}_h, \mathbf{u}_h)\big\}$.

Consider the finite element discretization of (3) using the pair of conforming finite element spaces $V_h \subset V$ and $Q_h \subset Q$ that satisfy the inf-sup compatibility condition

$$\inf_{q_h\in Q_h}\sup_{\mathbf{v}_h\in V_h}\frac{(\nabla\cdot\mathbf{v}_h, q_h)}{\|\nabla\mathbf{v}_h\|_0\|q_h\|_0} \geq \beta > 0. \tag{4}$$

The finite element formulation of (3) reads: find $(\mathbf{u}_h, p_h) \in V_h \times Q_h$ such that for all $(\mathbf{v}_h, q_h) \in V_h \times Q_h$

$$\begin{cases} \nu(\nabla \mathbf{u}_h, \nabla \mathbf{v}_h) + b_s(\mathbf{b}; \mathbf{u}_h, \mathbf{v}_h) + \sigma(\mathbf{u}_h, \mathbf{v}_h) + \gamma(\nabla \cdot \mathbf{u}_h, \nabla \mathbf{v}_h) - (\nabla \cdot \mathbf{v}_h, p_h) = (\mathbf{f}, \mathbf{v}), \\ (\nabla \cdot \mathbf{u}_h, q_h) = 0, \end{cases} \tag{5}$$

where $\gamma \geq 0$ is a stabilization parameter and the corresponding term can be seen as adding a consistent term to the momentum equation, as in most of the finite element $\nabla \cdot \mathbf{u}_h \neq 0$, plays a role of penalty term in the mass conservation.

The grad-div stabilization can be used with any finite element and meshing choice. Our interest lies in the space of weakly differentiable point-wise divergence-free functions and discretely divergence-free functions that are, respectively, defined by

$$\begin{aligned} V_0 &= \left\{ \mathbf{v} \in H_0^1(\Omega)^d \ : \ \nabla \cdot \mathbf{v} = 0 \right\} \\ V_{0,h} &= \left\{ \mathbf{v}_h \in V_h \ : \ (\nabla \cdot \mathbf{v}_h, q_h) = 0, \quad \text{for all } q_h \in Q_h \right\}. \end{aligned}$$

Note that the discretely divergence-free function does not have to be divergence-free. This means that $V_{0,h} \not\subset V_0$ even if $V_h \subset V$. Since the divergence-free element may result in violation of the mass conservation. Their stability relies on the choice of finite element spaces and special mesh construction. To derive appropriate values of the stabilization parameter γ, the space of divergence-free and discretely divergence-free functions $V_{00,h} \subset V_{0,h} \cap V_0$ will be used with particular emphasis on whether the space $V_{00,h}$ possesses optimal approximation properties or not.

Definition 1 Consider a sequence of quasi-uniform meshes with characteristic mesh size h and the corresponding spaces $V_{00,h}$. If for all $v \in V_0 \cap H^{k+1}(\Omega)^d$ there exists a sequence of $v_h \in V_{00,h}$ such that

$$\|\nabla(\mathbf{v} - \mathbf{v}_h)\|_0 \leq C_{V_{00,h}} h^k |\mathbf{v}|_{k+1} \tag{6}$$

with $C_{V_{00,h}}$ independent of h, then the sequence of spaces $V_{00,h}$ is said to possess optimal approximation properties (w.r.t. the space V_0).

3 Velocity estimates and grad-div parameters

In this section, we present the main results of this paper. In particular, only the minimization of the $H^1(\Omega)$ error of the velocity is considered to study the optimality of the stabilization parameters.

Theorem 1 *Let $\mathbf{f} \in H^{-1}(\Omega)$ is given and $(\mathbf{u}, p)$ be the solution of the continuous problem (3) and $(\mathbf{u}_h, p_h)$ be the solution of the discrete problem (5). Then, the following estimate in the $L^2(\Omega)$-norm of the gradient of the velocity holds*

$$\begin{aligned} \|\nabla(\mathbf{u} - \mathbf{u}_h)\|_0^2 \leq & \inf_{\mathbf{w}_h \in V_{0,h}} \left\{ \mathcal{C}_g \|\nabla(\mathbf{u} - \mathbf{w}_h)\|_0^2 + \mathcal{C}_r \|\mathbf{u} - \mathbf{w}_h\|_0^2 + \mathcal{C}_d \|\nabla \cdot \mathbf{w}_h\|_0^2 \right\} \\ & + \mathcal{C}_p \inf_{q_h \in Q_h} \|p - q_h\|_0^2, \end{aligned} \tag{7}$$

where the constants $\mathcal{C}_g$, $\mathcal{C}_r$, $\mathcal{C}_d$, and $\mathcal{C}_p$ depend on the problem data and are defined as follows:

Case I *Consider $\sigma > 0$ and $b_s(\mathbf{b}; \mathbf{u}_h, \mathbf{v}_h) = (\mathbf{b} \cdot \nabla \mathbf{u}_h, \mathbf{v}_h)$ with $\nabla \cdot \mathbf{b} = 0$, then*

$$\mathcal{C}_g = 4 + \frac{2\|\mathbf{b}\|_\infty^2}{\nu\sigma}, \quad \mathcal{C}_r = \frac{2\sigma}{\nu}, \quad \mathcal{C}_d = \frac{2\gamma}{\nu}, \quad \mathcal{C}_p = \frac{2}{\nu\gamma}. \tag{8}$$

Similarly, for $b_s(\mathbf{b}; \mathbf{u}_h, \mathbf{v}_h) = \frac{1}{2}\big\{(\mathbf{b} \cdot \nabla \mathbf{u}_h, \mathbf{v}_h) - (\mathbf{b} \cdot \nabla \mathbf{v}_h, \mathbf{u}_h)\big\}$, one has

$$\mathcal{C}_g = \left(6 + \frac{\|\mathbf{b}\|_\infty^2}{\nu\sigma}\right), \quad \mathcal{C}_r = \left(\frac{4\sigma}{\nu} + \frac{2\|\mathbf{b}\|_\infty^2}{\nu^2}\right), \quad \mathcal{C}_d = \frac{4\gamma}{\nu}, \quad \mathcal{C}_p = \frac{4}{\nu\gamma}. \tag{9}$$

Case II *Let $\sigma = 0$. Then*

$$\mathcal{C}_g = \left(6 + \frac{C\|\mathbf{b}\|_\infty^2}{\nu^2}\right), \quad \mathcal{C}_r = 0, \quad \mathcal{C}_d = \frac{4\gamma}{\nu}, \quad \mathcal{C}_p = \frac{4}{\nu\gamma}. \tag{10}$$

Proof For arbitrary $\mathbf{w}_h \in V_{0,h}$, consider the error splitting

$$\mathbf{u} - \mathbf{u}_h = (\mathbf{u} - \mathbf{w}_h) + (\mathbf{w}_h - \mathbf{u}_h) := \boldsymbol{\eta} + \boldsymbol{\xi}_h. \tag{11}$$

Then, the triangular and Young's inequalities imply that

$$\|\nabla \mathbf{u} - \nabla \mathbf{u}_h\|_0^2 \le 2\|\nabla \boldsymbol{\eta}\|_0^2 + 2\|\nabla \boldsymbol{\xi}_h\|_0^2. \tag{12}$$

Subtracting (3) and (5) yields the error equation

$$\begin{aligned} &\nu(\nabla \boldsymbol{\xi}_h, \nabla \mathbf{v}_h) + b_s(\mathbf{b}; \boldsymbol{\xi}_h, \mathbf{v}_h) + \sigma(\boldsymbol{\xi}_h, \mathbf{v}_h) + \gamma(\nabla \cdot \boldsymbol{\xi}_h, \nabla \cdot \mathbf{v}_h) \\ &\quad = -\nu(\nabla \boldsymbol{\eta}, \nabla \mathbf{v}_h) - b_s(\mathbf{b}; \boldsymbol{\eta}, \mathbf{v}_h) - \sigma(\boldsymbol{\eta}, \mathbf{v}_h) - \gamma(\nabla \cdot \boldsymbol{\eta}, \nabla \cdot \mathbf{v}_h) + (p, \nabla \cdot \mathbf{v}_h). \end{aligned}$$

Now, setting $\mathbf{v}_h = \boldsymbol{\xi}_h$ and using $(\nabla \cdot \boldsymbol{\xi}_h, q_h) = 0$ for any $q_h \in Q_h$, one arrives at

$$\begin{aligned} &\nu\|\nabla \boldsymbol{\xi}_h\|_0^2 + \sigma\|\boldsymbol{\xi}_h\|_0^2 + \gamma\|\nabla \cdot \boldsymbol{\xi}_h\|_0^2 \\ &\quad = -\nu(\nabla \boldsymbol{\eta}, \nabla \boldsymbol{\xi}_h) - b_s(\mathbf{b}; \boldsymbol{\eta}, \boldsymbol{\xi}_h) - \sigma(\boldsymbol{\eta}, \boldsymbol{\xi}_h) \\ &\qquad -\gamma(\nabla \cdot \boldsymbol{\eta}, \nabla \cdot \boldsymbol{\xi}_h) + (p - q_h, \nabla \cdot \boldsymbol{\xi}_h). \end{aligned} \tag{13}$$

The terms on the right-hand side of (13) will be estimated separately. Applying the Cauchy-Schwarz inequality and Young's inequality, one gets

$$\begin{aligned} \nu\|\nabla \boldsymbol{\xi}_h\|_0^2 + \sigma\|\boldsymbol{\xi}_h\|_0^2 + \gamma\|\nabla \cdot \boldsymbol{\xi}_h\|_0^2 \le{}& \nu\|\nabla \boldsymbol{\eta}\|_0^2 + \sigma\|\boldsymbol{\eta}\|_0^2 + \gamma\|\nabla \cdot \boldsymbol{\eta}\|_0^2 \\ &+ 2\big|b_s(\mathbf{b}; \boldsymbol{\eta}, \boldsymbol{\xi}_h)\big| + 2\big|(p - q_h, \nabla \cdot \boldsymbol{\xi}_h)\big|. \end{aligned} \tag{14}$$

The estimate of the last term on the right-hand side of (13) uses again the Cauchy-Schwarz and Young's inequalities, that is,

$$2\big|(p-q_h,\nabla\cdot\boldsymbol{\xi}_h)\big| \le 2\gamma^{-1/2}\,\|p-q_h\|_0\,\gamma^{1/2}\,\|\nabla\cdot\boldsymbol{\xi}_h\|_0 \le \gamma^{-1}\|p-q_h\|_0^2+\gamma\|\nabla\cdot\boldsymbol{\xi}_h\|_0^2 \tag{15}$$

for all $q_h \in Q_h$. For the estimate of the convective term, two different cases of σ are taken into account with the different representations of the bilinear form b_s. First, consider the case $\sigma > 0$. One get, respectively,

$$2\big|b_s(\mathbf{b};\boldsymbol{\eta},\boldsymbol{\xi}_h)\big| = 2\big|(\mathbf{b}\cdot\nabla\boldsymbol{\eta},\boldsymbol{\xi}_h)\big| \le 2\|\mathbf{b}\|_\infty\|\nabla\boldsymbol{\eta}\|_0\|\boldsymbol{\xi}_h\|_0 \le \frac{\|\mathbf{b}\|_\infty^2}{\sigma}\|\nabla\boldsymbol{\eta}\|_0^2+\sigma\|\boldsymbol{\xi}_h\|_0^2 \tag{16}$$

and

$$\begin{aligned}2\big|b_s(\mathbf{b};\boldsymbol{\eta},\boldsymbol{\xi}_h)\big| &= \big|(\mathbf{b}\cdot\nabla\boldsymbol{\eta},\boldsymbol{\xi}_h)-(\mathbf{b}\cdot\nabla\boldsymbol{\xi}_h,\boldsymbol{\eta})\big|\\ &\le \|\mathbf{b}\|_\infty\,\|\nabla\boldsymbol{\eta}\|_0\,\|\boldsymbol{\xi}_h\|_0+\|\mathbf{b}\|_\infty\,\|\nabla\boldsymbol{\xi}_h\|_0\|\boldsymbol{\eta}\|_0\\ &\le \frac{\|\mathbf{b}\|_\infty^2}{4\sigma}\|\nabla\boldsymbol{\eta}\|_0^2+\sigma\|\boldsymbol{\xi}_h\|_0^2+\frac{\|\mathbf{b}\|_\infty^2}{2\nu}\|\boldsymbol{\eta}\|_0^2+\frac{\nu}{2}\|\nabla\boldsymbol{\xi}_h\|_0^2.\end{aligned} \tag{17}$$

Inserting (15) and (16) into (14), one arrives at

$$\|\nabla\boldsymbol{\xi}_h\|_0^2 \le \left(1+\frac{\|\mathbf{b}\|_\infty^2}{\nu\sigma}\right)\|\nabla\boldsymbol{\eta}\|_0^2+\frac{\sigma}{\nu}\|\boldsymbol{\eta}\|_0^2+\frac{\gamma}{\nu}\|\nabla\cdot\boldsymbol{\eta}\|_0^2+\frac{1}{\nu\gamma}\inf_{q_h\in Q_h}\|p-q_h\|_0^2.$$

Hence, expression (12) implies

$$\begin{aligned}&\|\nabla(\mathbf{u}-\mathbf{u}_h)\|_0^2\\ &\le 4\left(1+\frac{\|\mathbf{b}\|_\infty^2}{2\nu\sigma}\right)\|\nabla\boldsymbol{\eta}\|_0^2+\frac{2\sigma}{\nu}\|\boldsymbol{\eta}\|_0^2+\frac{2\gamma}{\nu}\|\nabla\cdot\boldsymbol{\eta}\|_0^2+\frac{2}{\nu\gamma}\inf_{q_h\in Q_h}\|p-q_h\|_0^2,\end{aligned}$$

which gives (7) together with the constants defined in (8).

Substituting the estimates from (15) and (17) into (14), it can be seen that

$$\begin{aligned}\|\nabla\boldsymbol{\xi}_h\|_0^2 \le{}& 2\|\nabla\boldsymbol{\eta}\|_0^2+\frac{2\sigma}{\nu}\|\boldsymbol{\eta}\|_0^2+\frac{2\gamma}{\nu}\|\nabla\cdot\boldsymbol{\eta}\|_0^2+\frac{\|\mathbf{b}\|_\infty^2}{2\nu\sigma}\|\nabla\boldsymbol{\eta}\|_0^2+\frac{\|\mathbf{b}\|_\infty^2}{\nu^2}\|\boldsymbol{\eta}\|_0^2\\ &+\frac{2}{\nu\gamma}\inf_{q_h\in Q_h}\|p-q_h\|_0^2,\end{aligned}$$

which, together with expression (12), yields

$$\begin{aligned}\|\nabla(\mathbf{u}-\mathbf{u}_h)\|_0^2 \le{}& \left(6+\frac{\|\mathbf{b}\|_\infty^2}{\nu\sigma}\right)\|\nabla\boldsymbol{\eta}\|_0^2+\left(\frac{4\sigma}{\nu}+\frac{2\|\mathbf{b}\|_\infty^2}{\nu^2}\right)\|\boldsymbol{\eta}\|_0^2+\frac{4\gamma}{\nu}\|\nabla\cdot\boldsymbol{\eta}\|_0^2\\ &+\frac{4}{\nu\gamma}\inf_{q_h\in Q_h}\|p-q_h\|_0^2,\quad\forall\mathbf{w}_h\in V_{0,h}.\end{aligned}$$

This renders the estimate (7) with the constants defined in (9).

Consider now the second case where $\sigma = 0$. Applying Hölder's inequality followed by the Poincaré and Young's inequalities, one gets the estimate of the convective term

$$b_s(\mathbf{b};\boldsymbol{\eta},\boldsymbol{\xi}_h) \leq C\|\mathbf{b}\|_\infty \|\nabla\boldsymbol{\eta}\|_0 \|\nabla\boldsymbol{\xi}_h\|_0 \leq \frac{C\|\mathbf{b}\|_\infty^2}{\nu}\|\nabla\boldsymbol{\eta}\|_0^2 + \frac{\nu}{4}\|\nabla\boldsymbol{\xi}_h\|_0^2.$$

Using the aforementioned inequality, $\sigma = 0$, and (15) into the estimate (14) to get

$$\|\nabla\boldsymbol{\xi}_h\|_0^2 \leq \left(2 + \frac{C\|\mathbf{b}\|_\infty^2}{\nu^2}\right)\|\nabla\boldsymbol{\eta}\|_0^2 + \frac{2\gamma}{\nu}\|\nabla\cdot\boldsymbol{\eta}\|_0^2 + \frac{2}{\gamma\nu}\inf_{q_h\in Q_h}\|p - q_h\|_0^2.$$

Finally, the prove is completed by using this estimate in (12) and defining the constants as in (10). □

Remark 1 The analysis presented above can be extended to the steady-state Navier-Stokes equations. To this end, considering the decomposition (11), the error equation (13) becomes

$$\begin{aligned}\nu\|\nabla\boldsymbol{\xi}_h\|_0^2 + \gamma\|\nabla\cdot\boldsymbol{\xi}_h\|_0^2 = -\nu(\nabla\boldsymbol{\eta},\nabla\boldsymbol{\xi}_h) - \gamma(\nabla\cdot\boldsymbol{\eta},\nabla\cdot\boldsymbol{\xi}_h) + (p - q_h, \nabla\cdot\boldsymbol{\xi}_h)\\ - b_s(\mathbf{u};\mathbf{u},\boldsymbol{\xi}_h) + b_s(\mathbf{u}_h,\mathbf{u}_h,\boldsymbol{\xi}_h).\end{aligned}$$

The first three terms can be estimated in a similar way as for the Oseen equations. The estimate for the trilinear terms, which can be written as

$$b_s(\mathbf{u};\mathbf{u},\boldsymbol{\xi}_h) - b_s(\mathbf{u}_h,\mathbf{u}_h,\boldsymbol{\xi}_h) = b_s(\mathbf{u};\boldsymbol{\eta},\boldsymbol{\xi}_h) + b_s(\boldsymbol{\eta};\mathbf{u}_h,\boldsymbol{\xi}_h) - b_s(\boldsymbol{\xi}_h;\mathbf{u}_h,\boldsymbol{\xi}_h),$$

follows from standard finite element analysis of the Navier-Stokes equations. However, the estimate of the last term on the right-hand side requires an assumption on the smallness of the data. Altogether, one obtains the following estimate

$$\begin{aligned}&\|\nabla(\mathbf{u} - \mathbf{u}_h)\|_0^2\\ &\quad\leq C\left\{\|\nabla\boldsymbol{\eta}\|_0^2 + \frac{\gamma}{\nu}\|\nabla\cdot\boldsymbol{\eta}\|_0^2 + \frac{1}{\nu\gamma}\inf_{q_h\in Q_h}\|p - q_h\|_0^2 + \left(1 + \frac{1}{\nu^4}\|\mathbf{f}\|_{H^{-1}(\Omega)}\right)\|\nabla\boldsymbol{\eta}\|_0^2\right\}.\end{aligned}$$

Remark 2 The assumption on the convection field $\mathbf{b} \in L^\infty(\Omega)^d$ is standard in analysis of the Oseen problem [16]. On the other hand, if $\mathbf{b} \in H^1(\Omega)^d$, then the estimate of the convective term using $\nabla\cdot\mathbf{b} = 0$ becomes

$$\begin{aligned}2\left|b_s(\mathbf{b},\boldsymbol{\eta},\boldsymbol{\xi}_h)\right| &\leq C\|\mathbf{b}\|_0^{1/2}\|\mathbf{b}\|_1^{1/2}\|\nabla\boldsymbol{\eta}\|_0\|\nabla\boldsymbol{\xi}_h\|_0\\ &\leq C\frac{\|\mathbf{b}\|_0\|\mathbf{b}\|_1}{\nu}\|\nabla\boldsymbol{\eta}\|_0^2 + \frac{\nu}{2}\|\nabla\boldsymbol{\xi}_h\|_0^2.\end{aligned}$$

The second term on the right hand-side of above estimate can be hidden in the left-hand side of (14). Comparing the last estimate with (16), we have $C\|\mathbf{b}\|_0\|\mathbf{b}\|_1/\nu$ instead of

$\|\mathbf{b}\|_\infty^2/\sigma$. Hence, one get the optimal estimate (7) with lower regularity assumption and the constants are given by

$$\mathcal{C}_g = 6 + \frac{C\|\mathbf{b}\|_0\|\mathbf{b}\|_1}{\nu^2}, \quad \mathcal{C}_r = \frac{4\gamma}{\nu}, \quad \text{or} \quad \mathcal{C}_r = 0 \quad \text{if } \sigma = 0, \quad \mathcal{C}_d = \frac{4}{\nu\gamma}.$$

Remark 3 Assume that $1/h < \sigma$. Using an inverse inequality, one obtains an alternative estimate for the convective term

$$\begin{aligned}
&2\left|b_s(\mathbf{b};\boldsymbol{\eta},\boldsymbol{\xi}_h)\right| \\
&\quad = \left|(\mathbf{b}\cdot\nabla\boldsymbol{\eta},\boldsymbol{\xi}_h) - (\mathbf{b}\cdot\nabla\boldsymbol{\xi}_h,\boldsymbol{\eta})\right| \le \|\mathbf{b}\|_\infty\,\|\nabla\boldsymbol{\eta}\|_0\,\|\boldsymbol{\xi}_h\|_0 + \|\mathbf{b}\|_\infty\,\|\nabla\boldsymbol{\xi}_h\|_0\|\boldsymbol{\eta}\|_0 \\
&\quad \le \|\mathbf{b}\|_\infty\|\nabla\boldsymbol{\eta}\|_0\|\boldsymbol{\xi}_h\|_0 + \|\mathbf{b}\|_\infty c_{\text{inv}}h^{-1}\|\boldsymbol{\xi}_h\|_0\|\boldsymbol{\eta}\|_0 \\
&\quad \le \frac{\|\mathbf{b}\|_\infty^2}{2\sigma}\|\nabla\boldsymbol{\eta}\|_0^2 + \sigma\|\boldsymbol{\xi}_h\|_0^2 + \frac{\|\mathbf{b}\|_\infty^2 c_{\text{inv}}^2}{2\sigma h^2}\|\boldsymbol{\eta}\|_0^2.
\end{aligned}$$

Together with (12), (14), and (15), the statement of the Theorem 1 follows with the constants

$$\mathcal{C}_g = \left(4 + \frac{\|\mathbf{b}\|_\infty^2}{\sigma\nu}\right), \quad \mathcal{C}_r = \left(\frac{2\sigma}{\nu} + \frac{\|\mathbf{b}\|_\infty^2 c_{\text{inv}}^2}{\sigma\nu h^2}\right), \quad \mathcal{C}_d = \frac{2\gamma}{\nu}, \quad \mathcal{C}_p = \frac{2}{\nu\gamma}.$$

In practice, $\mathcal{C}_r$ contains a constant c_{inv} which is not exactly known and it is for uniform grids. Therefore, it is not considered in the forthcoming analysis.

Remark 4 Note that the error bound (7) is only for the gradient of the velocity. One can easily extend it to the case where the left-hand side of (7) can be expressed as a linear combination of three errors for the velocity, i.e.,

$$\begin{aligned}
&\nu\|\nabla(\mathbf{u}-\mathbf{u}_h)\|_0^2 + \sigma\|\mathbf{u}-\mathbf{u}_h\|_0^2 + \gamma\|\nabla\cdot(\mathbf{u}-\mathbf{u}_h)\|_0^2 \\
&\quad \le \inf_{\mathbf{w}_h\in V_{0,h}}\left\{\mathcal{C}_g\|\nabla(\mathbf{u}-\mathbf{w}_h)\|_0^2 + \mathcal{C}_r\|\mathbf{u}-\mathbf{w}_h\|_0^2 + \mathcal{C}_d\|\nabla\cdot\mathbf{w}_h\|_0^2\right\} \\
&\qquad + \mathcal{C}_p\inf_{q_h\in Q_h}\|p-q_h\|_0^2,
\end{aligned}$$

where the constants on the right-hand side are different from those in Theorem 1.

As pointed out in the grad-div stabilization applied to the Stokes problem [19], the key point of the analysis consists in tracking the divergence error to the final estimate of Theorem 1. This allows to study the consequences of the error bounds (7) on the choice of the parameter γ for the case of point-wise divergence-free subspace of the velocity space with or without optimal approximation properties.

3.1 Taylor-Hood elements

Corollary 1 *Consider* $(V_h, Q_h) = \left((P_k)^d, P_{k-1}\right)$ *on quasi-uniform meshes and* $(\mathbf{u}, p) \in H^{k+1}(\Omega)^d \times H^k(\Omega)$.

The estimates are distinguished into different categories depending on the existence of the optimal approximation properties.

Case 1 First consider the general case where the space $V_{00,h}$ does not have the optimal approximation properties. In this case, the estimate of Theorem 1 take the form

$$\|\nabla \mathbf{u} - \nabla \mathbf{u}_h\|_0^2 \leq \left[\mathcal{C}_g + \mathcal{C}_r h^2 + \mathcal{C}_d\right] C_{V_{0,h}}^2 h^{2k} |\mathbf{u}|_{k+1}^2 + \mathcal{C}_p C_{Q_h}^2 h^{2k} |p|_k^2. \tag{18}$$

Case 2 If the space $V_{00,h}$ has the optimal approximation properties, the estimate (7) gives

$$\begin{aligned}\|\nabla \mathbf{u} - \nabla \mathbf{u}_h\|_0^2 \leq \min \left\{ \left[\left[\mathcal{C}_g + \mathcal{C}_r h^2 + \mathcal{C}_d\right] C_{V_{0,h}}^2, \mathcal{C}_g + \mathcal{C}_r h^2\right] C_{V_{00,h}}^2 \right\} h^{2k} |\mathbf{u}|_{k+1}^2 \\ + \mathcal{C}_p C_{Q_h}^2 h^{2k} |p|_k^2.\end{aligned} \tag{19}$$

Here, the constants $\mathcal{C}_g$, $\mathcal{C}_r$, $\mathcal{C}_d$, and $\mathcal{C}_p$ appearing on the right-hand side of (18) and (19) are defined in (8)–(10) for appropriate cases and the constants C_{Q_h}, $C_{V_0,h}$ and $C_{V_{00,h}}$ are the interpolation estimate constants.

Proof The proof follows the same argument as in [19, Corollary 1]. □

In the remainder of this section, two cases will be discussed in detail. Firstly, we consider the case when the space $V_{00,h}$ does not have optimal approximation properties. In this case, one can regard the right-hand side of (18) as a function depending on γ. This function attains minimum which can be determined by elementary calculus

$$\gamma_{\text{opt}} \approx \frac{C_{Q_h} |p|_k}{C_{V_{0,h}} |\mathbf{u}|_{k+1}}. \tag{20}$$

Note that the parameter γ_{opt} is similar to the one that is obtained for the Stokes problem [19], and, with respect to ν and h, the standard parameter choice $\gamma = \mathcal{O}(1)$ is recovered. Inserting γ_{opt} into (18), leads to

$$\|\nabla(\mathbf{u} - \mathbf{u}_h)\|_0 \leq h^k \left(\left(\mathcal{C}_g + \mathcal{C}_r h^2\right) C_{V_{0,h}}^2 |\mathbf{u}|_{k+1}^2 + \frac{2\varepsilon}{\nu} C_{V_{0,h}} C_{Q_h} |\mathbf{u}|_{k+1} |p|_k \right)^{1/2} \tag{21}$$

with $\varepsilon = 2$ or 4 depending on different cases in Theorem 1.

Consider now the case where the space $V_{00,h}$ has optimal approximation properties. In order to obtain good value of parameter γ, let us follow the criterion for the case of Stokes problem, that is, consider the contribution of the pressure error equal to the maximum possible contribution of the velocity error. This criterion for the estimate (19) leads to

$$\gamma_{\text{good}} \approx \frac{\varepsilon C_{Q_h}^2 |p|_k^2}{\nu \left(\mathcal{C}_g + \mathcal{C}_r h^2\right) C_{V_{00,h}}^2 |\mathbf{u}|_{k+1}^2}. \tag{22}$$

It is interesting to note that the γ_{good} is ν-dependent. Moreover, from the definitions of the constants in (8) and (9), it can be seen that the γ_{good} also depends on σ. The

dependence of σ and ν can also be observed in the numerical simulations. Inserting (22) into (19) gives

$$\|\nabla(\mathbf{u}-\mathbf{u}_h)\|_0 \leq \varepsilon \left(\mathcal{C}_g + \mathcal{C}_r h^2\right)^{1/2} C_{V_{00,h}} h^k |\mathbf{u}|_{k+1} \tag{23}$$

with $\varepsilon = \sqrt{8}$ or $\sqrt{2}$ depending on $\sigma = 0$ or $\sigma > 0$, respectively. For estimates (21) and (23), since $\mathcal{C}_g$ and $\mathcal{C}_r$ depend on ν^{-1} (even ν^{-2} when $\sigma = 0$), one expect to see an increase of the error for small viscosities. Furthermore, one does not observe a dependence on the mesh width in both cases.

3.2 Mini elements

It is well known that the use of equal-order finite element pair $((P_k)^d, P_k)$ does not satisfy the inf-sup condition (4). In order to overcome the difficulty, a PSPG term have to be added to the discrete formulation (5), see e.g., [2,21]. The use of MINI element (P_k^{bub}, P_k) is equivalent to applying the PSPG stabilization, with a special choice of the PSPG parameter [22].

Corollary 2 *Consider* $(V_h, Q_h) = \left((P_k^{\text{bub}})^d, P_k\right)$ *on quasi-uniform meshes and* $(\mathbf{u}, p) \in H^{k+1}(\Omega)^d \times H^{k+1}(\Omega)$.

Similarly as for the Taylor-Hood element, two cases depending on the the approximation properties of the space $V_{00,h}$ *are detailed in the following.*

Case 1 A-priori estimate (7), for the general case where the space $V_{00,h}$ *does not have optimal approximation properties, has the form*

$$\|\nabla(\mathbf{u}-\mathbf{u}_h)\|_0^2 \leq \left[\mathcal{C}_g + h^2\mathcal{C}_r + \mathcal{C}_d\right] C_{V_{0,h}}^2 h^{2k} |\mathbf{u}|_{k+1}^2 + \mathcal{C}_p C_{Q_h}^2 h^{2k+2} |p|_{k+1}^2. \tag{24}$$

Case 2 In the case that the space $V_{00,h}$ *has optimal approximation properties, the a-priori estimate (7) becomes*

$$\begin{aligned}\|\nabla(\mathbf{u}-\mathbf{u}_h)\|_0^2 \leq \min &\left\{\left[\left(\mathcal{C}_g + \mathcal{C}_r h^2 + \mathcal{C}_d\right) C_{V_{0,h}}^2, \mathcal{C}_g + \mathcal{C}_r h^2\right] C_{V_{00,h}}^2\right\} h^{2k} |\mathbf{u}|_{k+1}^2 \\ &+ \mathcal{C}_p C_{Q_h}^2 h^{2k+2} |p|_{k+1}^2\end{aligned} \tag{25}$$

with $\mathcal{C}_g$, $\mathcal{C}_r$, $\mathcal{C}_d$ *and* $\mathcal{C}_p$ *from Theorem 1. Note that, in both estimates, there is a dependence of the parameters on the mesh width* h *which comes from the equal-order finite element pairs of velocity and pressure.*

Using the same idea as in the Taylor-Hood element for finding the parameters γ_{opt} and γ_{good}, depending on the approximation properties of the space $V_{00,h}$, one arrives at

$$\gamma_{\text{opt}} = \frac{h C_{Q_h} |p|_{k+1}}{C_{V_{0,h}} |\mathbf{u}|_{k+1}}, \quad \gamma_{\text{good}} = \frac{\varepsilon h^2 C_{Q_h}^2 |p|_{k+1}^2}{\nu \left(\mathcal{C}_g + \mathcal{C}_r h^2\right) C_{V_{00,h}}^2 |\mathbf{u}|_{k+1}^2}. \tag{26}$$

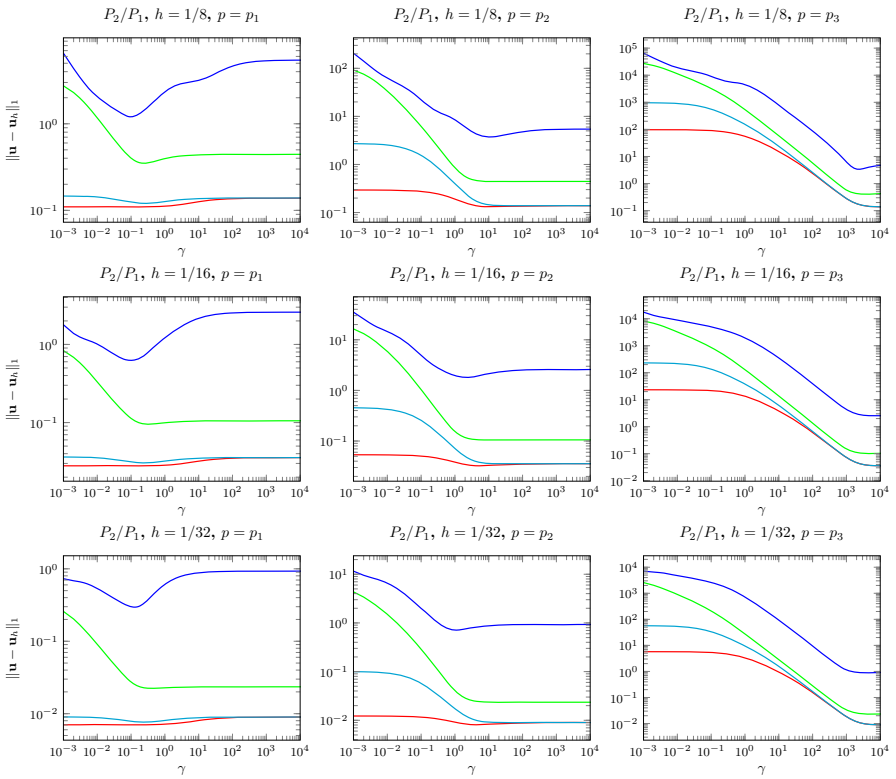

Fig. 1 Errors in the H^1-norm of velocity vs. grad-div stabilization parameter γ with $\sigma = 0$ using the Taylor-Hood element on successive refinements of barycenter–refined uniform meshes

In these cases, one expect a dependence of the optimal γ on the mesh width h. Inserting γ_{opt} and γ_{good} into (24) and (25), respectively, gives the following estimates

$$\|\nabla(\mathbf{u} - \mathbf{u}_h)\|_0 \leq h^k \left(\left(\mathcal{C}_g + h^2 \mathcal{C}_r \right) C_{V_{0,h}}^2 |\mathbf{u}|_{k+1}^2 + \frac{2h\varepsilon}{\nu} C_{V_{0,h}} C_{Q_h} |p|_{k+1} |\mathbf{u}|_{k+1} \right)^{1/2} \tag{27}$$

and

$$\|\nabla(\mathbf{u} - \mathbf{u}_h)\|_0 \leq \varepsilon h^k \left(\mathcal{C}_g + h^2 \mathcal{C}_r \right)^{1/2} C_{V_{0,h}} |\mathbf{u}|_{k+1}. \tag{28}$$

A similar observation as for the Taylor-Hood element can be made for the MINI element, that is, a decrease in the viscosity would lead to a large velocity errors, since the constant $\mathcal{C}_g$ and $\mathcal{C}_r$ depend on ν^{-1}.

4 Numerical studies

This section presents the numerical results consisting of two examples. In the first example, Ω is considered to be the unit square $(0, 1)^2$, in which the analytic solution is known. In this example, our interest lies in computing and comparing the influence

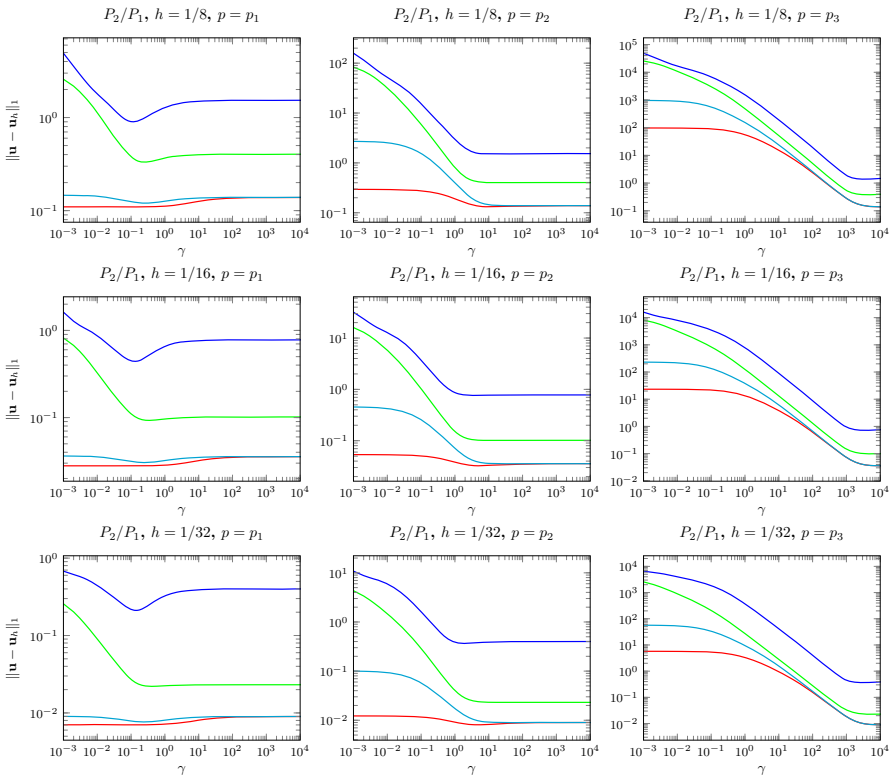

Fig. 2 Errors in the H^1-norm of velocity vs. grad-div stabilization parameter γ with $\sigma = 1$ using the Taylor-Hood element on successive refinements of barycenter–refined uniform meshes

of the optimal γ with the theoretical results presented in previous section. The second example is the well known steady-state flow past a circular cylinder. The goal of this example is to numerically investigate the effect of the parameter γ in grad-div stabilization applied to Navier-Stokes equation. All numerical simulations were performed with the finite element code MooNMD [23].

4.1 Example with known analytic solution

Consider the problem (2) on $\Omega = (0, 1)^2$, $\mathbf{b} = \mathbf{u}$ and $\sigma \geq 0$. Choose $\mathbf{f}$ and the boundary conditions such that

$$\mathbf{u}(\mathbf{x}, \mathbf{y}) = \begin{pmatrix} \cos(2\pi \mathbf{y}) \\ \sin(2\pi \mathbf{x}) \end{pmatrix}$$

and three different pressure solutions which serve as pressure field

$$p_1 = \sin(2\pi \mathbf{y}), \quad p_2 = \sin(8\pi \mathbf{y}), \quad p_3 = 10^4 \sin(2\pi \mathbf{y}).$$

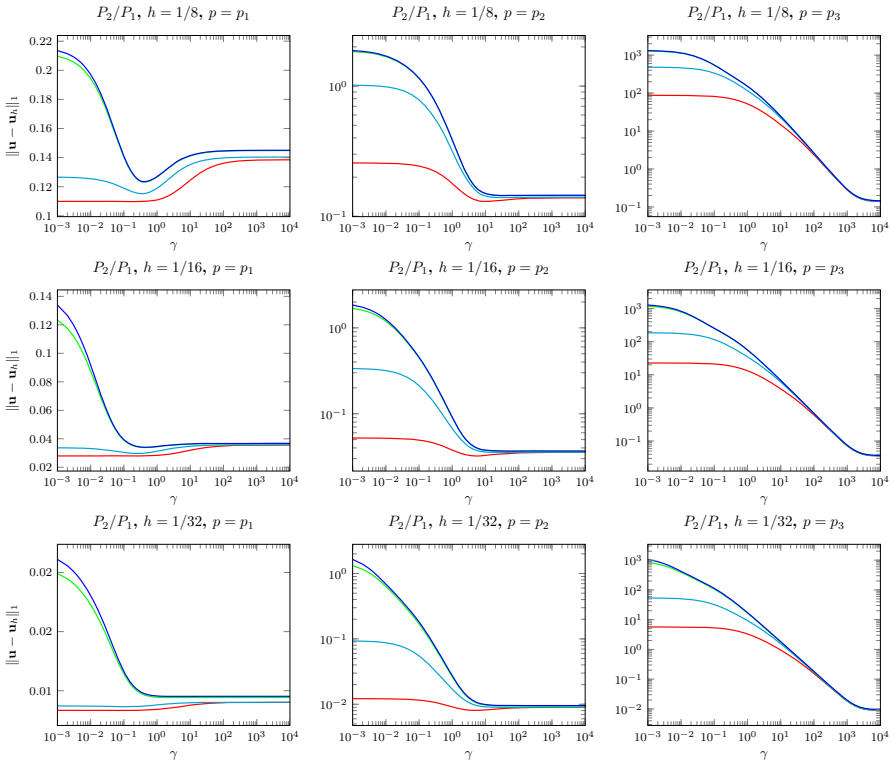

Fig. 3 Errors in the H^1-norm of velocity vs. grad-div stabilization parameter γ with $\sigma = 500$ using the Taylor-Hood element on successive refinements of barycenter–refined uniform meshes

Note that, for each pressure function, the source term is different. In the numerical studies, the viscosity $\nu \in \{1, 10^{-1}, 10^{-3}, 10^{-6}\}$ is used and the stabilization parameter γ varies in a wide range from 10^{-3} to 10^4.

For the case where the point-wise divergence-free subspace of the velocity space has optimal approximation properties, we use the scaling factor $\theta_{\nu,h}$ defined by

$$\theta_{\nu,h} = \begin{cases} 4/(4\nu + 2/\sigma + 2\sigma h^2) & \text{if } \sigma > 0, \\ 4/(6\nu + h^2/\nu) & \text{if } \sigma = 0, \end{cases} \tag{29}$$

which is derived from (8) and (10).

In order to compare the results with the Stokes problem [19], numerical studies for this example are performed on uniformly refined grids using the Taylor-Hood element and the MINI element [24]. It is known from [25] that the point-wise divergence-free subspace $(P_2)^2$ of the velocity space has optimal approximation properties on the barycenter-refined mesh. Also, the point-wise divergence-free subspace of $\left(P_1^{\text{bub}}\right)^2$ on union jack type meshes has optimal approximation properties.

Table 1 Optimal values of γ and the H^1 velocity error corresponding to Fig. 1

ν	$p = p_1$			$p = p_2$			$p = p_3$		
	γ	Min	Std.	γ	Min	Std.	γ	Min	Std.
$h = 1/8$									
— 1	0.062	1.098e−1	1.116e−1	12	1.313e−1	1.906e-01	10,000	1.379e−1	5.598e1
— 1e−1	0.620	1.204e−1	1.263e−1	68	1.388e−1	3.974e-01	10,000	1.385e−1	1.531e2
— 1e−3	0.240	3.499e−1	3.960e−1	17	4.410e−1	8.569e-01	3400	4.076e−1	5.382e2
— 1e−6	0.100	1.202e−1	2.337	11	3.743e−1	8.497	2300	3.378e−1	4.503e3
$h = 1/16$									
— 1	0.042	2.795e−2	2.842e−2	5.7	3.238e−2	3.816e−2	10,000	3.554e−2	1.355e1
— 1e−1	0.25	3.050e−2	3.210e−2	33	3.556e−2	7.135e−2	10,000	3.560e−2	3.797e1
— 1e−3	0.32	9.539e−2	9.947e−2	12	1.048e−1	1.547e−1	5200	1.019e−1	1.295e2
— 1e−6	0.098	6.257e−1	1.215	2.1	1.803412	1.960	8400	2.544	1.952e3
$h = 1/32$									
— 1	0.035	7.026e−3	7.143e−3	4.9	8.081e−3	9.137e−3	10,000	8.960e−3	3.345
— 1e−1	0.25	7.654e−3	8.062e−3	38	8.972e−3	1.734e−2	10,000	8.965e−3	9.467
— 1e−3	0.4	2.240e−2	2.276e−2	36	2.348e−2	4.081e−2	6600	2.310e−2	2.741e1
— 1e−6	0.13	2.958e−1	6.098e−1	1.1	7.149e−1	7.153e−1	3800	8.922e−1	7.161e2

Table 2 Optimal values of γ and the H^1 velocity error corresponding to Fig. 2

ν	$p = p_1$			$p = p_2$			$p = p_3$		
	γ	Min	Std.	γ	Min	Std.	γ	Min	Std.
$h = 1/8$									
— 1	0.059	1.098e−1	1.116e−1	12	1.313e−1	1.906e−1	10,000	1.385e−1	5.5971
— 1e−1	0.26	1.203e−1	1.262e−1	68	1.388e−1	3.972e−1	10,000	1.391e−1	1.5302
— 1e−3	0.25	3.314e−1	3.666e−1	18	4.012e−1	8.085e−1	3900	3.809e−1	4.8242
— 1e−6	0.11	9.010e−1	1.288	12	1.504	2.975	3000	1.385	1.5323
$h = 1/16$									
— 1	0.042	2.795e−2	2.842e−2	5.7	3.238e−2	3.816e−2	10,000	3.554e−2	1.3551
— 1e−1	0.25	3.050e−2	3.210e−2	33	3.556e−2	7.134e−2	10,000	3.560e−2	3.7971
— 1e−3	0.33	9.285e−2	9.635e−2	12	1.012e−1	1.514e−1	5600	9.881e−2	1.2502
— 1e−6	0.13	4.418e−1	6.551e−1	39	7.635e−1	8.658e−1	3100	7.214e−1	7.7952
$h = 1/32$									
— 1	0.035	7.026e−3	7.143e−3	4.9	8.081e−3	9.137e−3	10,000	8.960e−3	3.345
— 1e−1	0.25	7.654e−3	8.062e−3	38	8.973e−3	1.734e−2	10,000	8.965e−3	9.467
— 1e−3	0.41	2.207e−2	2.241e−2	36	2.310e−2	4.046e−2	6700	2.273e−2	2.719e1
— 1e−6	0.14	2.110e−1	3.248e−1	1.9	3.683e−1	3.876e−1	2600	3.669e−1	3.702e2

Table 3 Optimal values of γ and the H^1 velocity error corresponding to Fig. 3

ν	$p = p_1$			$p = p_2$			$p = p_3$		
	γ	Min	Std.	γ	Min	Std.	γ	Min	Std.
$h = 1/8$									
— 1	0.19	1.097e−1	1.098e−1	11	1.298e−1	2.431954e−1	10,000	1.386e−1	8.146e1
— 1e−1	0.35	1.152e−1	1.189e−1	31	1.393e−1	7.824974e−1	10,000	1.405e−1	3.374e2
— 1e−3	0.42	1.231e−1	1.404e−1	44	1.443e−1	1.143	10,000	1.449e−1	5.444e2
— 1e−6	0.42	1.233e−1	1.411e−1	44	1.445e−1	1.150	10,000	1.451e−1	5.484e2
$h = 1/16$									
— 1	0.077	2.794e−2	2.794e−2	5.6	3.224e−2	4.937e−2	10,000	3.554e−2	2.113e1
— 1e−1	0.26	2.966e−2	3.042e−2	24	3.547e−2	2.117e−1	10,000	3.561e−2	1.157e2
— 1e−3	0.44	3.381e−2	3.903e−2	62	3.661e−2	4.453e−1	10,000	3.657e−2	2.493e2
— 1e−6	0.46	3.402e−2	3.943e−2	63	3.675e−2	4.542e−1	10,000	3.672e−2	2.535e2
$h = 1/32$									
— 1	0.001	8.339e−3	8.341e−3	4.9	8.071e−3	1.158e−2	10,000	8.959e−3	5.290
— 1e−1	0.11	8.646e−3	8.647e−3	34	8.966e−3	5.491e−2	10,000	8.964e−3	3.206e1
— 1e−3	3.1	9.420e−3	1.142e−2	220	9.401e−3	1.699e−1	10,000	9.363e−3	1.056e2
— 1e−6	3.3	9.521e−3	1.164e−2	220	9.554e−3	1.817e−1	10,000	9.526e−3	1.125e2

For simplicity of presentation, the parameters proposed by the theoretical results in previous section are denoted by γ_{good} and the optimal γ corresponds to the best results obtained in the numerical simulations.

4.1.1 $((P_2)^2, P_1)$ *Taylor-Hood element on barycenter-refined grids*

First consider the Taylor-Hood element on the barycentric refined uniform mesh, where the divergence-free subspace of the velocity space possesses optimal approximation properties. In this case, (20) is taken into account and a good choice of γ satisfies

$$\gamma_{\text{good}} \approx \theta_{\nu,h} C_0 \frac{|p|_2^2}{|\mathbf{u}|_3^2} = \theta_{\nu,h} C_0 \begin{cases} \frac{1}{2\pi^2} & \text{for } p = p_1, \\ \frac{128}{\pi^2} & \text{for } p = p_2, \\ \frac{10^8}{2\pi^2} & \text{for } p = p_3, \end{cases} \tag{30}$$

where C_0 is an unknown interpolation constant, which is independent of h and γ. For each simulation, after having found the optimal parameter, one can compute an estimate of these constant. Here and in the following sections, for the sake of brevity, we skip the calculation of these constants, see [19] for details. The simulations were performed on three barycenter-refined triangular meshes with $h \in \{1/8, 1/16, 1/32\}$.

Numerical results are presented in Figs. 1, 2 and 3 for the constant $\sigma = 0, 1$ and 500, respectively. The curves in these figures plots the $H^1(\Omega)$ velocity error against the grad-div stabilization parameter γ. Also in Tables 1, 2 and 3, the corresponding actual

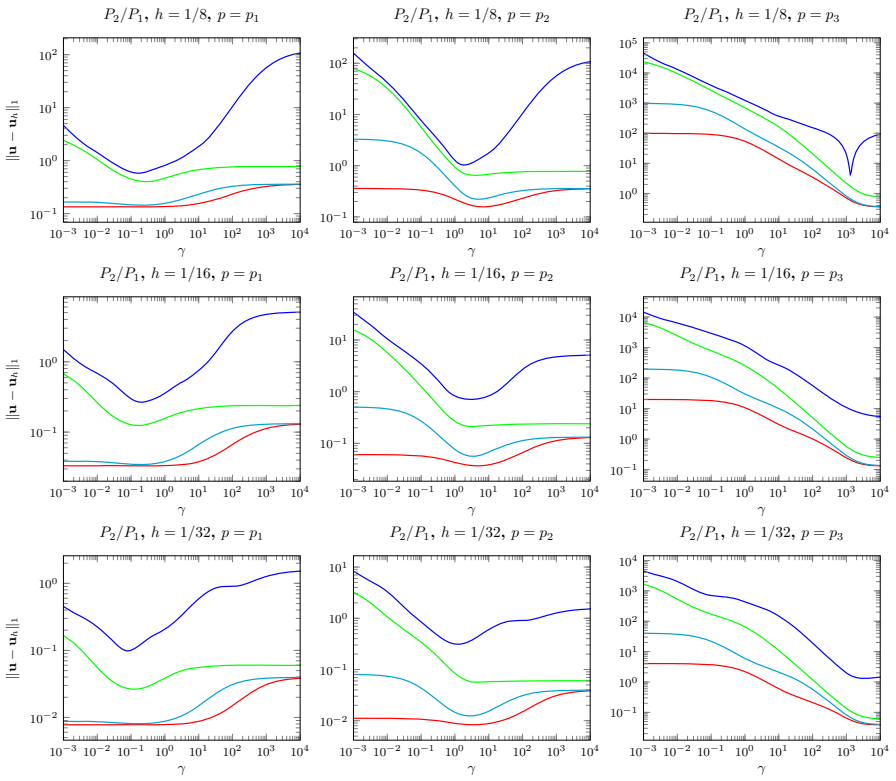

Fig. 4 Errors in the H^1-norm of velocity vs. grad-div stabilization parameter γ with $\sigma = 0$ using the Taylor-Hood element on successive refinements of Delaunay generated triangulations

optimal parameter γ and the $H^1(\Omega)$ velocity error for standard choice $\gamma = 1$ (std) are given. Note that, the constant $\theta_{v,h}$ in (29) is a linear combination of the viscosity ν, the reaction term σ, and the mesh width h or only of the viscosity and mesh width. Hence, the situation is different for different values of these constants. Consider the case when $\sigma = 0$, one expect a decrease in the optimal γ for large viscosity whereas it decreases when the viscosity becomes smaller. This behavior can be seen in Fig. 1 and Table 1. On the other hand, for $\sigma > 0$, an increase in the optimal parameter for the large values of ν but weak or almost no dependence of γ on ν can be observed from (29). This expectation can be well observed always for $\sigma = 500$, see Fig. 3 and Table 3. For $\sigma = 1$, the increase of optimal γ can be seen in Fig. 2 and Table 2, but the situation of constant γ is not reached. Also it should be noted that, for all viscosity (especially for $\nu = 10^{-3}$ and 10^{-6}), the error is always almost constant in a wide range of γ. In such a situation, small changes of the velocity errors due to round-off errors might become important for the determination of the optimal stabilization parameter.

The next prediction from (30) that the γ increases notably if $|p|_2^2|$ increases. This effect is well observed in all simulations by comparing the values of the parameter γ for p_1 and p_2 (similarly for p_2 and p_3). The independence of the optimal parameter

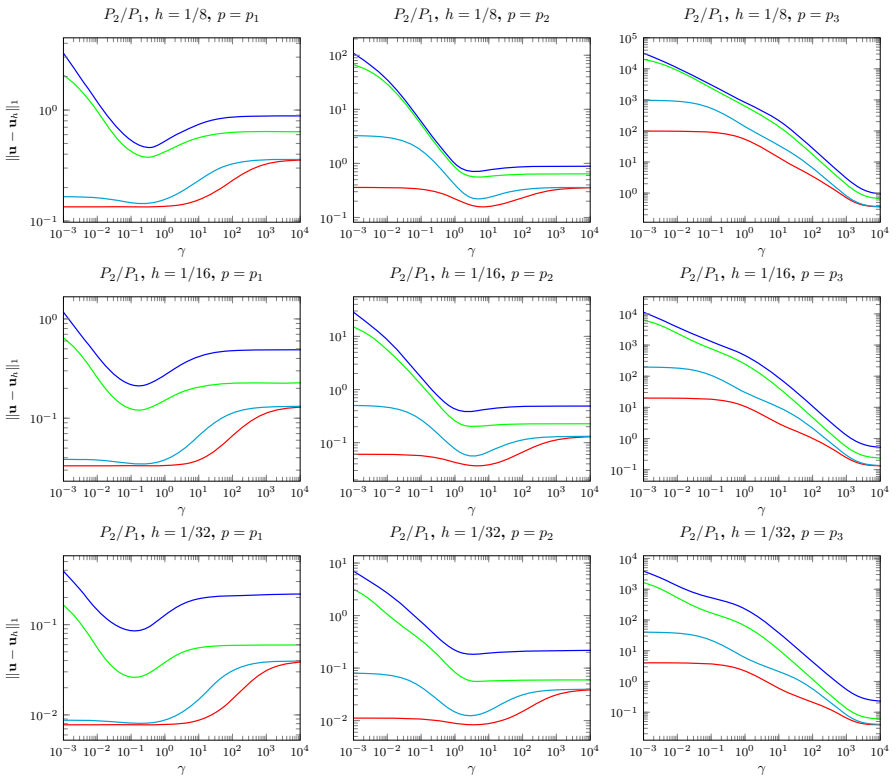

Fig. 5 Errors in the H^1-norm of velocity vs. grad-div stabilization parameter γ with $\sigma = 1$ using the Taylor-Hood element on successive refinements of Delaunay generated triangulations

γ on mesh width and very large optimal γ is predicted if $|p|_2^2$ is large. One can see that, both predictions are always met in numerical simulations as well.

Since inserting the values of the constants $\mathcal{C}_g$ and $\mathcal{C}_r$ into the error estimate (23) leads to the dependence on $\nu^{1/2}$ (or ν when $\sigma = 0$) of terms on the right-hand side of the estimate, one expects to see an increase of the error for the optimal stabilization parameter if ν decreases. This increase can be well observed for the cases when $\sigma = 0$ and $\sigma = 1$. For $\sigma = 500$, this increase is not very pronounced. We think that for the small values of the viscosities, the error from the grad-div contribution dominates the error contribution from the viscous term, see Remark 4.

With respect to the accuracy of the computed solution (similar to the Stokes problem [19]), one can clearly see for the large $|p|_2$ (i.e., for p_3) that the errors computed with the optimal γ are smaller by several order of magnitude than the errors obtained with the standard parameter $\gamma = 1$.

4.1.2 $((P_2)^2, P_1)$ Taylor-Hood element on Delaunay-generated triangulations

The consideration of the $((P_2)^2, P_1)$ Taylor-Hood element on a Delaunay-generated triangulation is considered in this section. In this case, the point-wise divergence-free

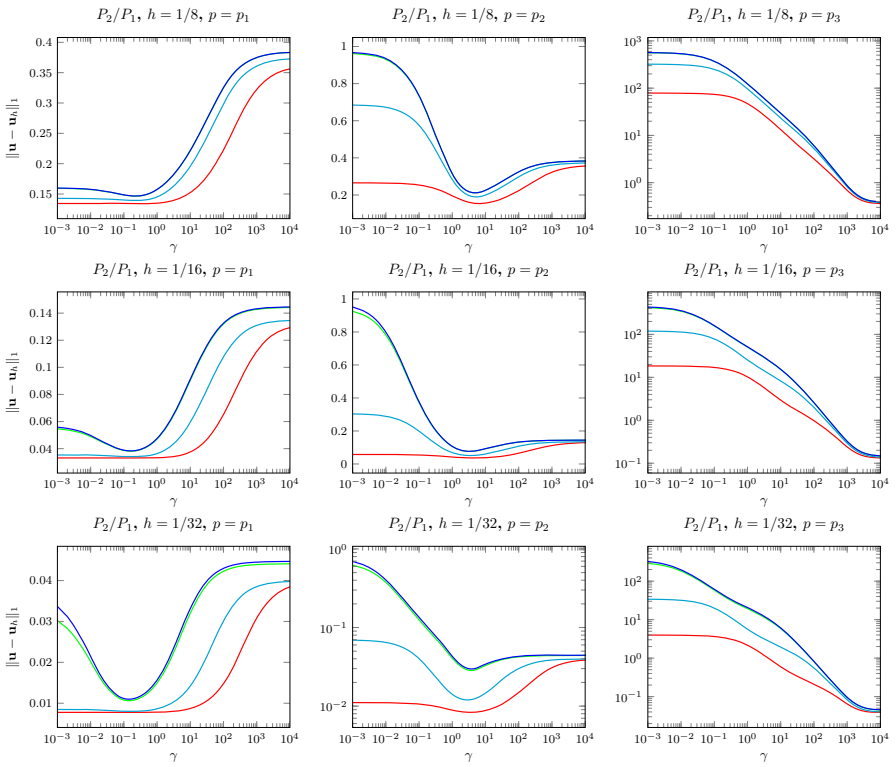

Fig. 6 Errors in the H^1-norm of velocity vs. grad-div stabilization parameter γ with $\sigma = 500$ using the Taylor-Hood element on successive refinements of Delaunay generated triangulations

subspace of the velocity space does not have the optimal approximation properties. Hence, the parameter choice (20) is applied which is similar to the γ_{good} for the Stokes problem, one obtains

$$\gamma_{\text{good}} \approx \begin{cases} \frac{C_0}{\sqrt{8\pi}} & \text{for } p = p_1, \\ \frac{C_0\sqrt{32}}{\pi} & \text{for } p = p_2, \\ \frac{C_0 10^4}{\sqrt{8\pi}} & \text{for } p = p_3. \end{cases} \tag{31}$$

The simulations were performed on three successively refined Delaunay-generated triangulations with $h \in \{1/8,\ 1/16,\ 1/32\}$.

The results of the numerical studies are presented in Figs. 4, 5 and 6, respectively for $\sigma = 0$, $\sigma = 1$, and $500\}$. The actual optimal parameter γ and the $H^1(\Omega)$ velocity errors are given in Tables 4, 5 and 6 for different mesh refinements. From (31), it is expected that the optimal γ is independent of the viscosities ν and the mesh width h. Both expectations were always in agreement with the theoretical prediction. It is further expected that the optimal γ is slightly increased between the pressure p_1 and p_2. Compared to the other case of a subspace with optimal approximation properties (Sect. 4.1.1), the increase should be smaller in the present case. This small

Table 4 Optimal values of γ and the H^1 velocity error corresponding to Fig. 4

ν	$p = p_1$			$p = p_2$			$p = p_3$		
	γ	Min	Std.	γ	Min	Std.	γ	Min	Std.
$h = 1/8$									
— 1	0.096	1.341e−1	1.353e−1	6.7	1.572e−1	2.218e−1	10,000	3.597e−1	5.397e1
— 1e−1	0.21	1.436e−1	1.566e−1	5.0	2.204e−1	4.012e−1	10,000	3.655e−1	1.391e2
— 1e−3	0.29	3.993e−1	4.674e−1	3.9	6.482e−1	9.341e−1	10,000	7.820e−1	6.955e2
— 1e−6	0.16	5.787e−1	8.137e−1	1.9	1.03079	1.268	1300	4.294	1.208e3
$h = 1/16$									
— 1	0.12	3.315e−2	3.333e−2	4.6	3.671e−2	4.273e−2	10,000	1.326e−1	1.071e1
— 1e−1	0.2	3.459e−2	3.801e−2	3.3	5.597e−2	7.658e−2	10,000	1.353e−1	3.028e1
— 1e−3	0.17	1.241e−1	1.571e−1	3.5	2.113e−1	2.661e−1	10,000	2.488e−1	2.542e2
— 1e−6	0.20	2.662e−1	3.567e−1	3.4	7.097e−1	8.181e−1	10,000	5.565	1.138e3
$h = 1/32$									
— 1	0.094	7.768e−3	7.809e−3	3.5	8.328e−3	8.903e−3	10,000	3.903e−2	2.191
— 1e−1	0.19	8.048e−3	8.760e−3	2.8	1.242e−2	1.461e−2	10,000	4.016e−2	6.018
— 1e−3	0.13	2.639e−2	3.873e−2	5.2	5.636e−2	8.425e−2	10,000	6.159e−2	6.527e1
— 1e−6	0.081	9.848e−2	2.078e−1	1.2	3.115e−1	3.146e−1	3100	1.313	4.357e2

Table 5 Optimal values of γ and the H^1 velocity error corresponding to Fig. 5

ν	$p = p_1$			$p = p_2$			$p = p_3$		
	γ	Min	Std.	γ	Min	Std.	γ	Min	Std.
$h = 1/8$									
— 1	0.096	1.341e−1	1.353e−1	6.7	1.572e−1	2.217e−1	10,000	3.597e−1	5.395e1
— 1e−1	0.21	1.435e−1	1.565e−1	5.0	2.202e−1	4.007e−1	10,000	3.654e−1	1.389e2
— 1e−3	0.31	3.755e−1	4.205e−1	4.7	5.597e−1	8.534e−1	10,000	6.630e−1	6.249e2
— 1e−6	0.33	4.577e−1	5.238e−1	3.8	7.090e−1	9.938e−1	10,000	9.391e−1	8.207e2
$h = 1/16$									
— 1	0.12	3.315e−2	1.353e−1	4.6	3.671e−2	2.217e−1	10,000	1.326e−1	5.395e1
— 1e−1	0.2	3.459e−2	1.565e−1	3.4	5.595e−2	4.007e−1	10,000	1.352e−1	1.389e2
— 1e−3	0.17	1.206e−1	4.205e−1	3.5	2.025e−1	8.534e−1	10,000	2.359e−1	6.248e2
— 1e−6	0.17	2.117e−1	5.238e−1	2.3	3.851e−1	9.938e−1	10,000	5.195e−1	8.207e2
$h = 1/32$									
— 1	0.092	7.768e−3	7.809e−3	3.5	8.328e−3	8.904e−3	10,000	3.903e−2	2.190
— 1e−1	0.19	8.048e−3	8.759e−3	2.8	1.242e−2	1.460e−2	10,000	4.016e−2	6.017
— 1e−3	0.13	2.607e−2	3.817e−2	5.2	5.560e−2	8.332e−2	10,000	6.080e−2	6.429e1
— 1e−6	0.13	8.495e−2	1.274e−1	3.3	1.832e−1	2.196e−1	10,000	2.304e−1	2.281e2

Table 6 Optimal values of γ and the H^1 velocity error corresponding to Fig. 5

ν	$p = p_1$			$p = p_2$			$p = p_3$		
	γ	Min	Std.	γ	Min	Std.	γ	Min	Std.
$h = 1/8$									
— 1	0.21	1.342e−1	1.342e−1	6.4	1.539e−1	2.539e−1	10,000	3.616e−1	7.368e1
— 1e−1	0.24	1.393e−1	1.401e−1	5.1	1.899e−1	5.753e−1	10,000	3.793e−1	2.499e2
— 1e−3	0.22	1.464e−1	1.484e−1	4.7	2.115e−1	7.315e−1	10,000	3.907e−1	3.684e2
— 1e−6	0.22	1.466e−1	1.485e−1	4.7	2.118e−1	7.340e−1	10,000	3.909e−1	3.704e2
$h = 1/16$									
— 1	0.13	3.314e−2	3.314e−2	4.6	3.651e−2	5.456e−2	10,000	1.327e−1	1.700e1
— 1e−1	0.20	3.408e−2	3.424e−2	3.5	5.114e−2	1.988e−1	10,000	1.382e−1	7.839e1
— 1e−3	0.16	3.818e−2	3.867e−2	3.2	7.575e−2	3.713e−1	10,000	1.480e−1	1.575e2
— 1e−6	0.16	3.839e−2	3.888e−2	3.2	7.653e−2	3.765e−1	10,000	1.484e−1	1.601e2
$h = 1/32$									
— 1	0.098	7.767e−3	7.767e−3	3.5	8.318e−3	1.061e−2	10,000	3.901e−2	3.650
— 1e−1	0.19	8.004e−3	8.051e−3	2.9	1.198e−2	4.020e−2	10,000	4.038e−2	1.995e1
— 1e−3	0.14	1.062e−2	1.077e−2	3.6	2.840e−2	1.250e−1	10,000	4.481e−2	5.824e1
— 1e−6	0.14	1.098e−2	1.114e−2	3.6	2.968e−2	1.346e−1	10,000	4.541e−2	6.149e1

increase is clearly visible in the numerical simulations. Moreover, much higher values of optimal parameter for the large $|p|_2$ (for p_3) can be seen, which are predicted by (31).

It is again clearly seen for large $|p|_2^2$ that the errors obtained by optimal γ are smaller by several order of magnitude compared to the errors obtained with standard $\gamma = 1$. From the estimate (21), it is expected that the error for the optimal parameter γ increases for small viscosities due to its dependence on $\nu^{-1/2}$. This effect can be well observed in the numerical simulations for $\sigma = 0$ and $\sigma = 1$, see Figs. 4, 5 and Tables 4, 5. The increase in the error is quite small for $\sigma = 500$, which might be because of the fact that contribution of the grad-div error dominates the error contribution of the viscous term for small viscosity, see Fig. 3 and Table 3.

4.1.3 The MINI element on union jack triangulations

Next, we consider the case of $\left((P_1^{\text{bub}})^2, P_1\right)$ MINI element on union jack type refined meshes. It is known from [26] that on this type of mesh the MINI element has the property that the point-wise divergence-free subspace of the velocity space has optimal approximation properties. In this case, the parameter choice (26) should be applied, such that

$$\gamma_{\text{good}} \approx \theta_{\nu,h} h^2 C_0 \frac{|p|_2^2}{|\mathbf{u}|_2^2} = \theta_{\nu,h} h^2 C_0 \begin{cases} 1/2 & \text{for } p = p_1, \\ 128 & \text{for } p = p_2, \\ 5 \cdot 10^7 & \text{for } p = p_3. \end{cases} \tag{32}$$

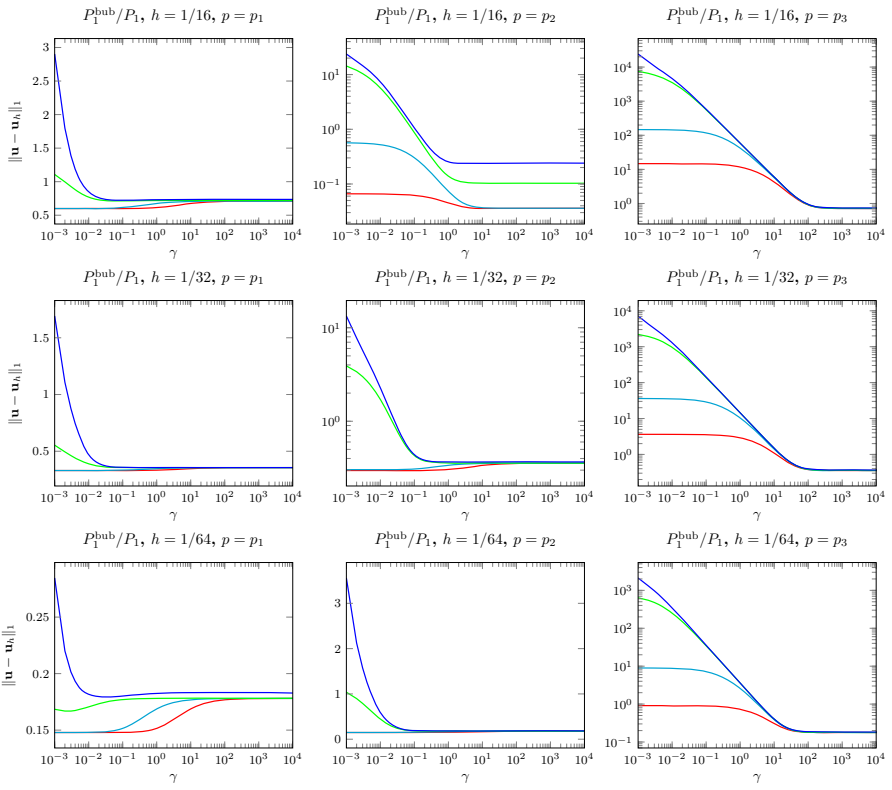

Fig. 7 Errors in the H^1-norm of velocity vs. grad-div stabilization parameter γ with $\sigma = 1$ using the MINI element on union jack triangulations with $h \in \{1/16,\ 1/32,\ 1/64\}$

For the sake of brevity, only results with $\sigma = 1$ and $\sigma = 500$ are presented. With $\sigma = 0$, almost similar results were obtained as for the case $\sigma = 0$. The numerical results were computed on three successively finer meshes of union jack type with $h \in \{1/16, 1/32, 1/64\}$.

The results for these numerical experiments are displayed in Figs. 7 and 8, and the corresponding optimal parameter γ and the $H^1(\Omega)$ velocity errors for the standard choice $\gamma = 1$ are given in Tables 7 and 8, respectively. The dependence of the optimal γ on the mesh width h, that is predicted by (32), can be clearly observed except for the case $\sigma = 1$ and $\nu = 10^{-6}$ with $p = p_1$, see Fig. 7 and Table 7. We think that the round-off errors influenced the simulations with small viscosities. A weak (or almost no) dependence of the optimal parameter γ on ν, which is predicted in (32), can be observed as well.

Finally, an increase of the error for small viscosities is expected from (28). One can in the numerical simulations that this increase is quite small. In addition, not that the error always stays constant on these meshes in a wide interval that also includes the optimal stabilization parameter γ.

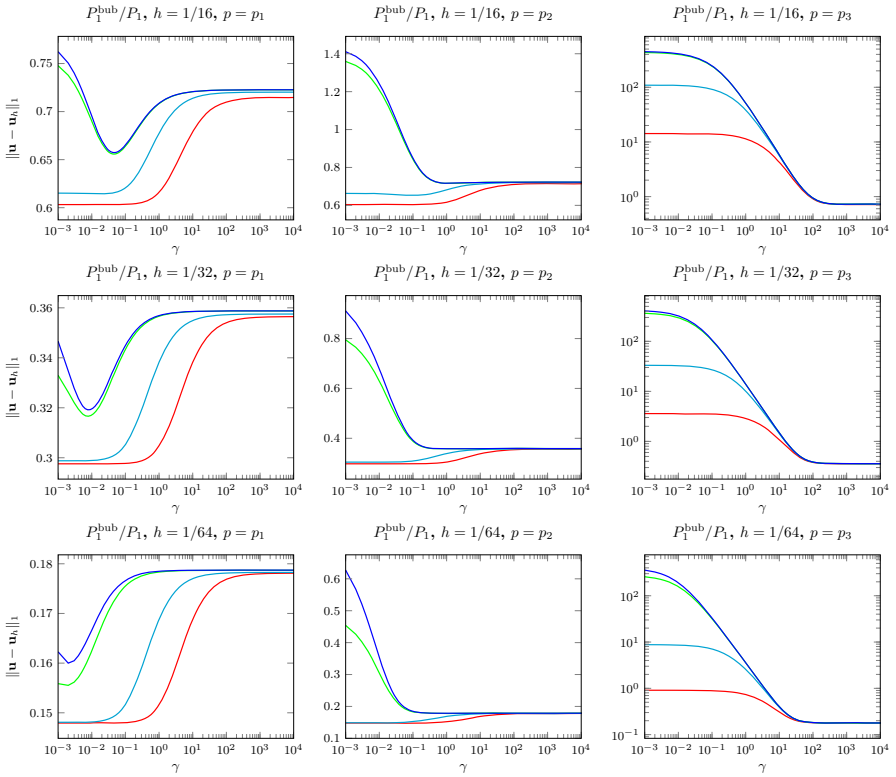

Fig. 8 Errors in the H^1-norm of velocity vs. grad-div stabilization parameter γ with $\sigma = 500$ using the MINI element on union jack triangulations with $h \in \{1/16, 1/32, 1/64\}$

4.1.4 The MINI element on Delaunay-generated triangulations

Finally, we consider the MINI element on Delaunay-generated triangulation where one does not expect the point-wise divergence-free subspace of velocity to have the optimal approximation properties. Hence, the stabilization parameter γ_{good} (26) will be taken into account, such that

$$\gamma_{\text{good}} \approx hC_0 \frac{|p|_2^2}{|\mathbf{u}|_2^2} = \begin{cases} \frac{C_0}{\sqrt{4}} h & \text{for } p = p_1, \\ 8\sqrt{2}\, C_0 h & \text{for } p = p_2, \\ 5000\sqrt{2}\, C_0 h & \text{for } p = p_3. \end{cases} \tag{33}$$

The results of the numerical studies are presented in Figs. 9 and 10 and the optimal parameter γ and the $H^1(\Omega)$ error are given in Tables 9 and 10. Again, one observes a decrease in the optimal γ with respect to the mesh h and a weak (or almost no) dependence on ν. Both predictions can be observed in the numerical simulation. A quite small increase of the error with respect to the viscosity can be be seen in the numerical simulations as well.

Table 7 Optimal values of γ and the H^1 velocity error corresponding to Fig. 7

ν	$p = p_1$			$p = p_2$			$p = p_3$		
	γ	Min	Std.	γ	Min	Std.	γ	Min	Std.
$h = 1/16$									
— 1	0.001	5.994e−1	6.129e−1	14	3.558e−2	4.504e−2	9700	7.104e−1	1.179e1
— 1e−1	0.001	5.998e−1	6.758e−1	130	3.606e−2	7.338e−2	10,000	7.105e−1	4.198e1
— 1e−3	0.067	7.128e−1	7.190e−1	51	1.031e−1	1.390e−1	10,000	7.203e−1	5.859e1
— 1e−6	0.091	7.222e−1	7.318e−1	3.4	2.369e−1	2.543e−1	10,000	7.358e−1	5.897e1
$h = 1/32$									
— 1	0.001	3.300e−1	3.330e−1	0.001	2.972e−1	3.042e−1	2300	3.559e−1	2.9073
— 1e−1	0.001	3.301e−1	3.463e−1	0.011	3.036e−1	3.381e−1	9800	3.559e−1	1.0329e1
— 1e−3	0.21	3.558e−1	3.558e−1	5.3	3.574e−1	3.579e−1	9900	3.574e−1	1.4399e1
— 1e−6	840	3.559e−1	3.561e−1	1.1	3.663e−1	3.663e−1	10,000	3.672e−1	1.4472e1
$h = 1/64$									
— 1	0.001	1.479e−1	1.515e−1	0.001	1.479e−1	1.516e−1	560	1.779e−1	7.353e−1
— 1e−1	0.001	1.479e−1	1.687e−1	0.002	1.486e−1	1.688e−1	5100	1.780e−1	2.575
— 1e−3	0.003	1.669e−1	1.781e−1	1.5	1.782e−1	1.782e−1	9600	1.782e−1	3.587
— 1e−6	0.033	1.794e−1	1.825e−1	0.43	1.823e−1	1.826e−1	10,000	1.828e−1	3.603

Table 8 Optimal values of γ and the H^1 velocity error corresponding to Fig. 8

ν	$p = p_1$			$p = p_2$			$p = p_3$		
	γ	Min	Std.	γ	Min	Std.	γ	Min	Std.
$h = 1/16$									
— 1	0.003	6.032e−1	6.035e−1	0.011	6.041e−1	6.043e−1	9400	7.148e−1	1.390e1
— 1e−1	0.018	6.145e−1	6.206e−1	0.11	6.527e−1	6.527e−1	10,000	7.202e−1	9.215e1
— 1e−3	0.046	6.557e−1	6.638e−1	1.2	7.158e−1	8.428e−1	10,000	7.226e−1	2.432e2
— 1e−6	0.046	6.573e−1	6.651e−1	1.2	7.162e−1	8.491e−1	10,000	7.226e−1	2.473e2
$h = 1/32$									
— 1	0.001	2.975e−1	2.977e−1	0.001	2.976e−1	2.978e−1	2300	3.564e−1	3.509
— 1e−1	0.001	2.987e−1	3.052e−1	0.009	3.043e−1	3.089e−1	9900	3.575e−1	2.703e1
— 1e−3	0.008	3.166e−1	3.433e−1	0.79	3.573e−1	3.882e−1	9900	3.587e−1	1.040e2
— 1e−6	0.008	3.191e−1	3.449e−1	0.91	3.577e−1	3.921e−1	10,000	3.587e−1	1.071e2
$h = 1/64$									
— 1	0.001	1.479e−1	1.480e−1	0.001	1.479e−1	1.480e−1	550	1.780e−1	8.880e−1
— 1e−1	0.001	1.480e−1	1.516e−1	0.002	1.487e−1	1.521e−1	5000	1.782e−1	7.073
— 1e−3	0.002	1.555e−1	1.755e−1	0.53	1.783e−1	1.830e−1	9900	1.786e−1	3.190e1
— 1e−6	0.002	1.599e−1	1.766e−1	0.83	1.785e−1	1.847e−1	9900	1.787e−1	3.307e1

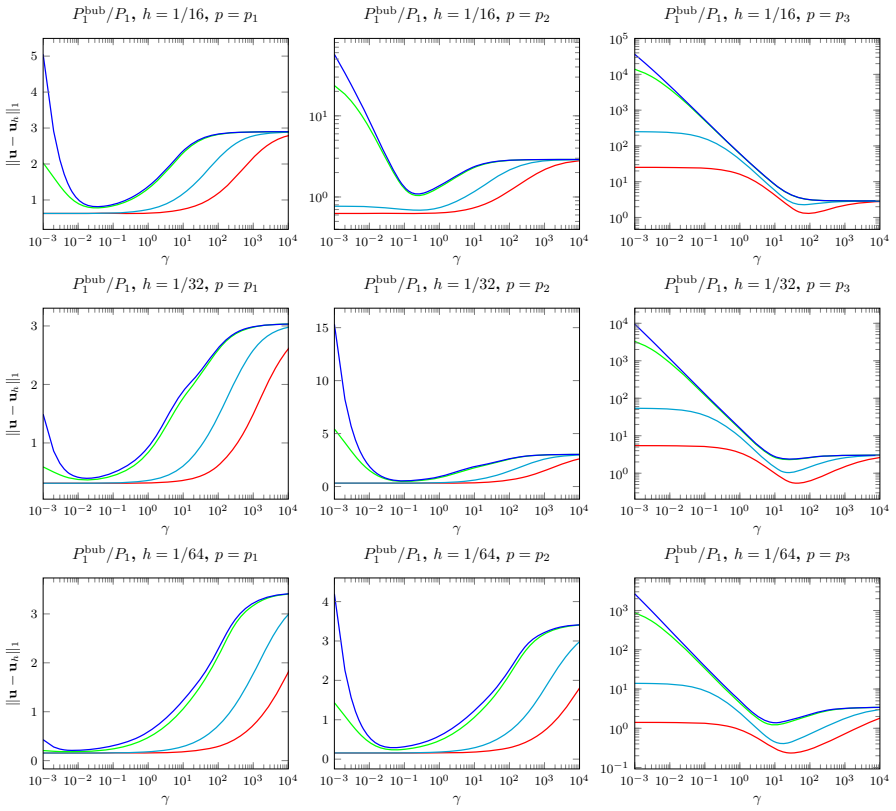

Fig. 9 Errors in the H^1-norm of velocity vs. grad-div stabilization parameter γ with $\sigma = 1$ using the MINI element on Delaunay-generated triangulations with $h \in \{1/16,\ 1/32,\ 1/64\}$

4.2 Steady-state flow around a cylinder

The second test problem is considered for the two-dimensional incompressible Navier-Stokes equations. The accuracy of the grad-div stabilization is studied numerically for the benchmark problem of channel flow past a cylinder, introduced in [27]. Figure 11 shows the geometry of the channel with the parabolic inflow is prescribed by

$$\mathbf{u}(0, \mathbf{y}) = 0.41^{-2}\big(1.2\mathbf{y}(0.41 - \mathbf{y}), 0\big), \quad 0 \le \mathbf{y} \le 0.41.$$

At the boundary $\mathbf{x} = 2.2$, the outflow condition $(\nu\nabla\mathbf{u} - pI)\mathbf{n} = 0$ is applied. In addition, homogeneous Dirichlet boundary conditions are enforced along the top and bottom walls. The viscosity is chosen to be $\nu = 10^{-3}$ and the source term $\mathbf{f} = 0$.

In order to study the accuracy of the grad-div stabilization method, the usual benchmark parameters [20] are the drag coefficient c_d at the cylinder and the lift coefficient c_ℓ, defined by

$$c_d = -500\big[(\nu\nabla\mathbf{u}, \nabla\mathbf{v}_d) + (\mathbf{u}\cdot\nabla\mathbf{u}, \mathbf{v}_d) - (p, \nabla\cdot\mathbf{v}_d)\big]$$

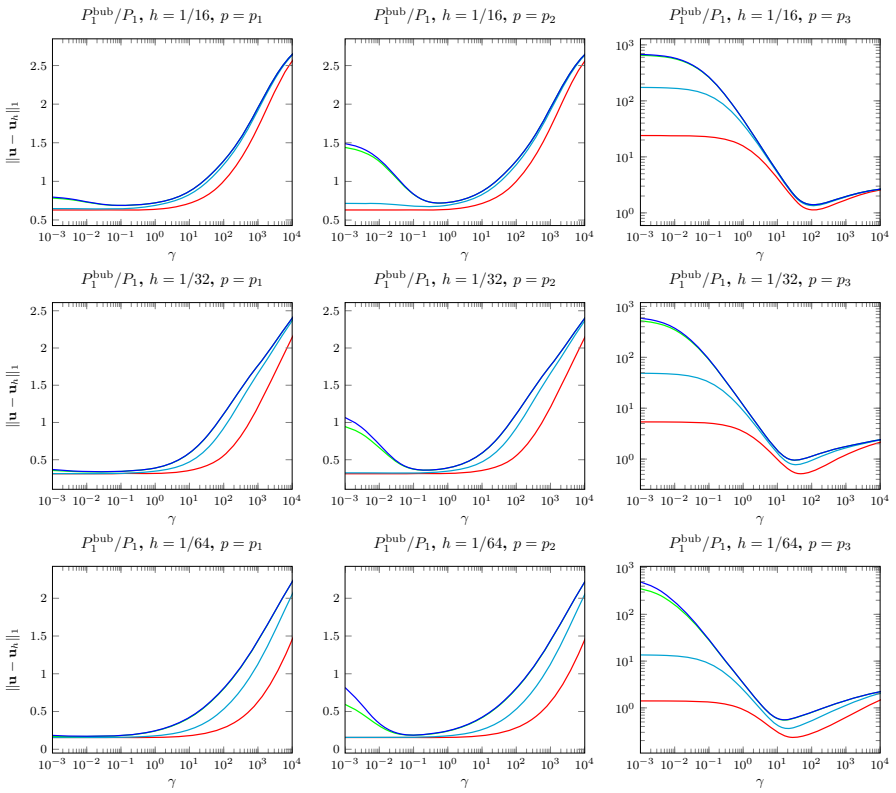

Fig. 10 Errors in the H^1-norm of velocity vs. grad-div stabilization parameter γ with $\sigma = 500$ using the MINI element on Delaunay-generated triangulations with $h \in \{1/16, 1/32, 1/64\}$

$$c_\ell = -500\big[(\nu\nabla\mathbf{u}, \nabla\mathbf{v}_\ell) + (\mathbf{u}\cdot\nabla\mathbf{u}, \mathbf{v}_\ell) - (p, \nabla\cdot\mathbf{v}_\ell)\big]$$

for any function $\mathbf{v}_d \in \big(H^1(\Omega)\big)^2$ with $(\mathbf{v}_d)\big|_S = (1,0)^T$, S being the boundary of the body and $\mathbf{v}_d$ vanishes on all other boundaries. The lift coefficient can be computed in a similar way by using $(\mathbf{v}_\ell)$ as a test function such that $(\mathbf{v}_\ell)\big|_S = (0,1)^T$ on the boundary of the cylinder. A third benchmark parameter is the difference of the pressure between the front and the back of the body

$$\Delta p = p(0.15, 0.2) - p(0.25, 0.2).$$

In the numerical simulations, the standard and Delaunay-generated triangulations are used. The initial grids are presented in Fig. 12, where the standard grid consists of 288 mesh cells and the Delaunay grid of 195 mesh cells. The Navier-Stokes equations were discretized by using the inf-sup stable pair of Taylor-Hood $((P_2)^2, P_1)$ and MINI $\big((P_1^{\text{bub}})^2, P_1\big)^2$ finite elements. The degrees of freedom for both elements on different refinement levels are given in table 11. The accuracy is measured with respect to the distance to the reference values, taken from [20],

Table 9 Optimal values of γ and the H^1 velocity error corresponding to Fig. 9

ν	$p = p_1$			$p = p_2$			$p = p_3$		
	γ	Min	Std.	γ	Min	Std.	γ	Min	Std.
$h = 1/16$									
— 1	0.001	6.248e−1	6.351e−1	0.041	6.263e−1	6.358e−1	860	1.29	1.611e1
— 1e−1	0.003	6.260e−1	7.353e−1	0.24	6.850e−1	7.395e−1	65	2.27	4.160e1
— 1e−3	0.033	7.801e−1	1.316	0.24	1.040	1.315	10,000	2.89	5.986e1
— 1e−6	0.035	8.142e−1	1.377	0.24	1.088	1.376	10,000	2.89	6.089e1
$h = 1/32$									
— 1	0.001	3.112e−1	3.158e−1	0.008	3.113e−1	3.159e−1	44	5.407e−1	3.512
— 1e−1	0.001	3.113e−1	3.594e−1	0.063	3.207e−1	3.599e−1	25	1.038	9.266
— 1e−3	0.017	3.686e−1	8.364e−1	0.10	4.840e−1	8.367e−1	25	2.299	1.507e1
— 1e−6	0.018	3.959e−1	9.284e−1	0.093	5.364e−1	9.280e−1	27	2.379	1.601e1
$h = 1/64$									
— 1	0.001	1.556e−1	1.580e−1	0.001	1.556e−1	1.580e−1	30	2.347e−1	9.233e−1
— 1e−1	0.001	1.556e−1	1.807e−1	0.017	1.571e−1	1.807e−1	17	4.081e−1	2.463
— 1e−3	0.007	1.798e−1	4.688e−1	0.054	2.362e−1	4.690e−1	97	1.221	4.411
— 1e−6	0.007	2.072e−1	5.889e−1	0.048	2.911e−1	5.893e−1	10	1.394	5.018

Table 10 Optimal values of γ and the H^1 velocity error corresponding to Fig. 10

ν	$p = p_1$			$p = p_2$			$p = p_3$		
	γ	Min	Std.	γ	Min	Std.	γ	Min	Std.
$h = 1/16$									
— 1	0.07	6.292e−1	6.292e−1	0.11	6.305e−1	6.305e−1	110	1.125	2.275e1
— 1e−1	0.05	6.431e−1	6.442e−1	0.27	6.728e−1	6.815e−1	110	1.346	1.247e2
— 1e−3	0.09	6.874e−1	6.875e−1	0.57	7.199e−1	8.317e−1	110	1.397	2.623e2
— 1e−6	0.1	6.890e−1	6.890e−1	0.58	7.206e−1	8.362e−1	110	1.398	2.655e2
$h = 1/32$									
— 1	0.017	3.117e−1	3.117e−1	0.022	3.118e−1	3.119e−1	49	5.148e−1	5.089
— 1e−1	0.011	3.133e−1	3.163e−1	0.067	3.206e−1	3.210e−1	35	7.760e−1	3.261e1
— 1e−3	0.015	3.350e−1	3.432e−1	0.23	3.596e−1	3.736e−1	33	9.520e−1	8.941e1
— 1e−6	0.019	3.383e−1	3.445e−1	0.23	3.606e−1	3.759e−1	33	9.551e−1	9.125e1
$h = 1/64$									
— 1	0.003	1.556e−1	1.557e−1	0.004	1.557e−1	1.557e−1	31	2.325e−1	1.333
— 1e−1	0.003	1.558e−1	1.580e−1	0.019	1.572e−1	1.586e−1	20	3.625e−1	8.917
— 1e−3	0.005	1.664e−1	1.812e−1	0.093	1.867e−1	1.867e−1	16	5.496e−1	2.806e1
— 1e−6	0.01	1.714e−1	1.830e−1	0.096	1.888e−1	1.888e−1	16	5.563e−1	2.884e1

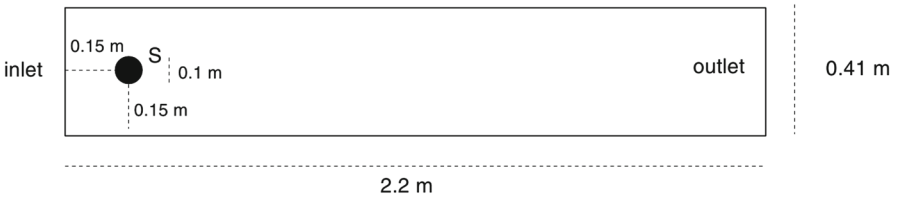

Fig. 11 Channel with cylinder

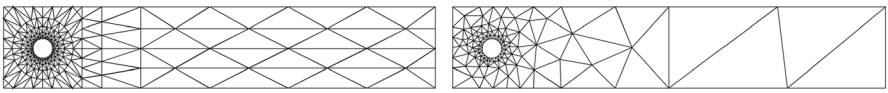

Fig. 12 Initial grids: standard *left* and Delaunay *right*

Table 11 DOF's

Level	$((P_2)^2, P_1)$	$\left((P_1^{\text{bub}})^2, P_1\right)^2$	
	Standard	Standard	Delaunay
2	7344	5684	2871
3	28,656	2210	11,202
4	113,184	87776	44,244

$$c_{\text{d,ref}} = 5.57953523384, \quad c_{\text{l,ref}} = 0.010618937712, \quad \Delta p_{\text{ref}} = 0.11752016697.$$

The simulations were performed on different levels of refinements that are presented in Fig. 13 for $\left((P_2)^2, P_1\right)$ on the standard grids and in Figs. 14 and 15 $\left((P_1)^{\text{bub}}, P_1\right)$ on the standard and Delaunay type grids, respectively. In particular, the errors of the computed values to the reference values are plotted along the varying grad-div stabilization parameter γ. Concerning the accuracy, the best results can be found with the smallest error.

From the numerical simulations, one can see that the optimal γ depends on the quantity of interest, i.e., drag or lift coefficients etc. Figure 13 for the Taylor-Hood element shows that the optimal γ should be smaller for the drag coefficient compared to the lift coefficient. Moreover, the optimal γ decreases for the drag coefficient, increases for the lift coefficient and pressure difference, with respect to the mesh width. This shows the dependency of the optimal γ on the mesh width h. One can see in plots of Fig. 13 that there are some pronounced peaks with very good results for small values of grad-div parameter, which are in agreement to the best results obtained with higher order finite elements in [20].

On the other hand, for the $\left((P_1)^{\text{bub}}, P_1\right)$ element (see Figs. 14, 15), one can conclude that the grad-div stabilization does not improve the accuracy of the computed solution. Comparing with the reference values one can see that the results are not accurate. In general, numerical simulations show that the results computed with the Taylor-Hood element are more accurate than with the MINI element. Finally, one can conclude from the experience of these simulations that although the predictions of the corresponding

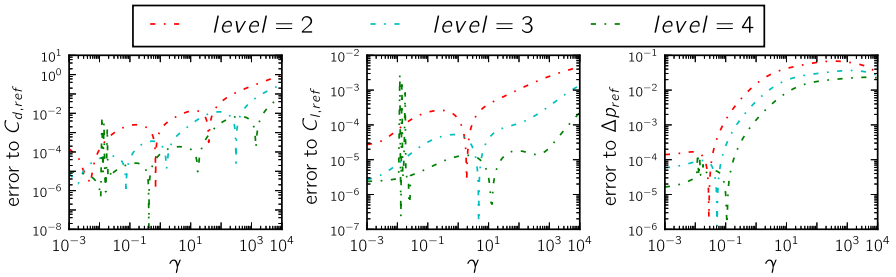

Fig. 13 Standard grid with $\left((P_2)^2, P_1\right)$ element: errors of the computed drag coefficient to $c_{\mathrm{d,ref}}$ (*left*), lift coefficient to $c_{\mathrm{l,ref}}$ (*middle*) and pressure difference to Δp_{ref} (*right*) vs. the grad-stabilization parameter γ on different refinement levels

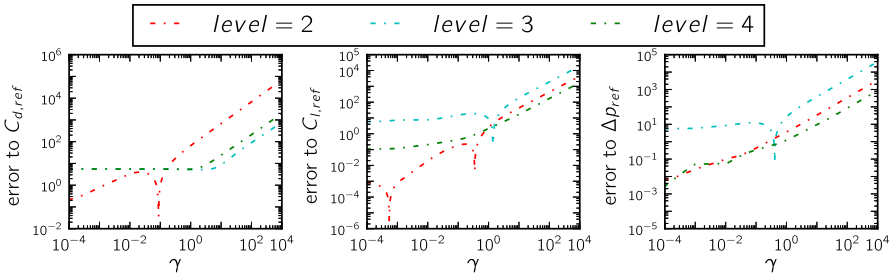

Fig. 14 Standard grid with $\left((P_1^{\mathrm{bub}})^2, P_1\right)$ element: error of the computed drag coefficient to $c_{\mathrm{d,ref}}$ (*left*), lift coefficient to $c_{\mathrm{l,ref}}$ (*middle*) and pressure difference to Δp_{ref} (*right*) vs. the grad-stabilization parameter γ on different refinement levels

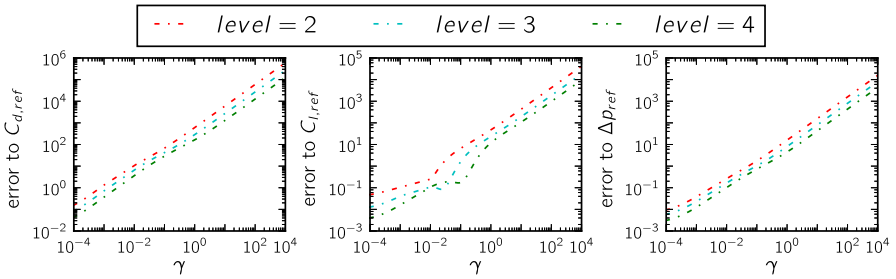

Fig. 15 Delaunay grid with $\left((P_1^{\mathrm{bub}})^2, P_1\right)$ element: error of the computed on drag coefficient to $c_{\mathrm{d,ref}}$ (*left*), lift coefficient to $c_{\mathrm{l,ref}}$ (*middle*) and pressure difference to Δp_{ref} (*right*) vs. the grad-stabilization parameter γ on different refinement levels

optimal parameter is impossible in practice, however the better results can be obtained with small parameter of the grad-div term.

5 Summary

This article provides a detailed study of the optimal grad-div stabilization parameter in finite element methods applied to the Oseen and Navier-Stokes equations. The

stabilization parameter for the Oseen equations is derived on the basis of minimizing the $H^1(\Omega)$ error of the velocity. From the theoretical estimates, it was noticed that the optimal parameter choice depends on the used norm, the solution, the finite element spaces, and the type of mesh. It was found that the special case of divergence-free velocity space with optimal approximation properties which leads for the Stokes equations to different grad-div parameters leads to the same parameter for Oseen equations. From a practical point of view, this observation is of advantage since in practice it is hard to decide which case is present. Since there is no difference in the parameter choice, one does not need to care for this issue. Because the reason for obtaining the same optimal parameters is the presence of the convective term in the Oseen equation, it can be expected that for the Navier-Stokes equations the same situation holds like for the Oseen equations.

On the other hand, it was observed both theoretically and numerically that the $H^1(\Omega)$ error of the velocity depends on the inverse of the viscosity parameter. Therefore the error increases by decreasing the viscosity. This observation holds irrespective of the optimal approximation properties of the divergence-free subspace of the velocity space.

With respect to the accuracy of the computed solution, it was shown that the errors computed with the optimal parameter are smaller by several order of magnitudes compared to the errors obtained with parameter of $\mathcal{O}(1)$.

Finally, in order to studying the impact of the grad-div stabilization to the Navier-Stokes equations, numerical tests are performed for a two-dimensional flow around a cylinder. It turns out for the Taylor-Hood element that the smaller values of the grad-div parameter lead to the best results. On the other hand, for the MINI element, accurate results can be obtained without grad-div stabilization.

Acknowledgements The author would like to thanks the unknown referees for their valuable suggestions and comments that helped to improve this paper.

References

1. Brooks, A.N., Hughes, T.J.R.: Streamline upwind/Petrov-Galerkin formulations for convection dominated flows with particular emphasis on the incompressible Navier-Stokes equations. Comput. Methods Appl. Mech. Eng. **32**(1–3), 199–259 (1982). [fENOMECH '81, Part I (Stuttgart, 1981)]
2. Franca, L.P., Frey, S.L.: Stabilized finite element methods. II. The incompressible Navier-Stokes equations. Comput. Methods Appl. Mech. Eng. **99**(2–3), 209–233 (1992)
3. Hansbo, P., Szepessy, A.: A velocity-pressure streamline diffusion finite element method for the incompressible Navier-Stokes equation. Comput. Methods Appl. Mech. Eng. **84**(2), 175–192 (1990)
4. Bazilevs, Y., Calo, V.M., Cottrell, J.A., Hughes, T.J.R., Reali, A., Scovazzi, G.: Variational multiscale residual-based turbulence modeling for large eddy simulation of incompressible flows. Comput. Methods Appl. Mech. Eng. **197**(1–4), 173–201 (2007)
5. Hughes, T.J.R., Feijóo, G.R., Mazzei, L., Quincy, J.-B.: The variational multiscale method—a paradigm for computational mechanics. Comput. Methods Appl. Mech. Eng. **166**(1–2), 3–24 (1998)
6. Olshanskii, M.A., Reusken, A.: Grad-div stabilization for Stokes equations. Math. Comp. **73**(248), 1699–1718 (2004)
7. Layton, W., Manica, C.C., Neda, M., Olshanskii, M., Rebholz, L.G.: On the accuracy of the rotation form in simulations of the Navier-Stokes equations. J. Comput. Phys. **228**(9), 3433–3447 (2009)
8. John, V., Kindl, A.: Numerical studies of finite element variational multiscale methods for turbulent flow simulations. Comput. Methods Appl. Mech. Eng. **199**(13–16), 841–852 (2010)

9. Matthies, G., Lube, G., Röhe, L.: Some remarks on residual-based stabilisation of inf-sup stable discretisations of the generalised Oseen problem. Comput. Methods Appl. Math. **9**(4), 368–390 (2009)
10. de Frutos, J., García-Archilla, B., John, V., Novo, J.: Grad-div stabilization for the evolutionary Oseen problem with inf-sup stable finite elements. J. Sci. Comput. **66**(3), 991–1024 (2016)
11. Dallmann, H., Arndt, D., Lube, G.: Local projection stabilization for the Oseen problem. IMA J. Numer. Anal. **36**(2), 796–823 (2016)
12. Heister, T., Rapin, G.: Efficient augmented Lagrangian-type preconditioning for the Oseen problem using grad-div stabilization. Int. J. Numer. Methods Fluids **71**(1), 118–134 (2013)
13. Börm, S., Le Borne, S.: $\mathscr{H}$-LU factorization in preconditioners for augmented Lagrangian and grad-div stabilized saddle point systems. Int. J. Numer. Methods Fluids **68**(1), 83–98 (2012)
14. Olshanskii, M., Lube, G., Heister, T., Löwe, J.: Grad-div stabilization and subgrid pressure models for the incompressible Navier-Stokes equations. Comput. Methods Appl. Mech. Eng. **198**(49–52), 3975–3988 (2009)
15. Olshanskii, M.A.: A low order Galerkin finite element method for the Navier-Stokes equations of steady incompressible flow: a stabilization issue and iterative methods. Comput. Methods Appl. Mech. Eng. **191**(47–48), 5515–5536 (2002)
16. Roos, H.-G., Stynes, M., Tobiska, L.: Robust numerical methods for singularly perturbed differential equations. Springer Series in Computational Mathematics, vol. 24, 2nd edn. Springer, Berlin (2008)
17. Braack, M., Burman, E., John, V., Lube, G.: Stabilized finite element methods for the generalized Oseen problem. Comput. Methods Appl. Mech. Eng. **196**(4–6), 853–866 (2007)
18. Galvin, K.J., Linke, A., Rebholz, L.G., Wilson, N.E.: Stabilizing poor mass conservation in incompressible flow problems with large irrotational forcing and application to thermal convection. Comput. Methods Appl. Mech. Eng. **237**(240), 166–176 (2012)
19. Jenkins, E.W., John, V., Linke, A., Rebholz, L.G.: On the parameter choice in grad-div stabilization for the Stokes equations. Adv. Comput. Math. **40**(2), 491–516 (2014)
20. John, V., Matthies, G.: Higher-order finite element discretizations in a benchmark problem for incompressible flows. Int. J. Numer. Methods Fluids **37**(8), 885–903 (2001)
21. Hughes, T.J.R., Franca, L.P., Balestra, M.: A new finite element formulation for computational fluid dynamics. V. Circumventing the Babuška-Brezzi condition: a stable Petrov-Galerkin formulation of the Stokes problem accommodating equal-order interpolations. Comput. Methods Appl. Mech. Eng. **59**(1), 85–99 (1986)
22. Pierre, R.: Simple C^0 approximations for the computation of incompressible flows. Comput. Methods Appl. Mech. Eng. **68**(2), 205–227 (1988)
23. John, V., Matthies, G.: MooNMD–a program package based on mapped finite element methods. Comput. Vis. Sci. **6**(2–3), 163–169 (2004)
24. Arnold, D.N., Brezzi, F., Fortin, M.: A stable finite element for theStokes equations. Calcolo **21**(4) 337–344 (1984)
25. Arnold, D.N., Jinshui, Q.: Quadratic velocity/linear pressure stokes elements. In: Advances in computer methods for partial differential equations VII, IMACS, pp. 28–34 (1992)
26. Zhang, S.: Bases for $C0-P1$ divergence-free elements and for $C1-P2$ finite elements on union jack grid (2012) (submitted)
27. Turek, S., Schäfer, M.: Benchmark computations of laminar flow around cylinder. In: Hirschel, E. (ed.) Flow simulation with high-performance computers II, vol. 52, pp. 547–566. Vieweg, Germany (1996)